

Efficient Deep Learning of Robust Policies from MPC using Imitation and Tube-Guided Data Augmentation

Andrea Tagliabue and Jonathan P. How

Abstract—Imitation Learning (IL) has been increasingly employed to generate computationally efficient policies from task-relevant demonstrations provided by Model Predictive Control (MPC). However, commonly employed IL methods are often data- and computationally-inefficient, as they require a large number of MPC demonstrations, resulting in long training times, and they produce policies with limited robustness to disturbances not experienced during training. In this work, we propose an IL strategy to *efficiently* compress a computationally expensive MPC into a deep neural network policy that is *robust* to previously unseen disturbances. By using a robust variant of the MPC, called Robust Tube MPC, and leveraging properties from the controller, we introduce a computationally-efficient data augmentation method that enables a significant reduction of the number of MPC demonstrations and training time required to generate a robust policy. Our approach opens the possibility of *zero-shot* transfer of a policy trained from a single MPC demonstration collected in a nominal domain, such as a simulation or a robot in a lab/controlled environment, to a new domain with previously unseen bounded model errors/perturbations. Numerical and experimental evaluations performed using linear and nonlinear MPC for agile flight on a multirotor show that our method outperforms strategies commonly employed in IL (such as Dataset-Aggregation (DAgger) and Domain Randomization (DR)) in terms of demonstration-efficiency, training time, and robustness to perturbations unseen during training.

Index Terms—Imitation Learning; Data Augmentation; Robust Tube Model Predictive Control; Aerial Robotics.

SUPPLEMENTARY MATERIAL

Video: <https://youtu.be/aWRuvy3LviI>.

I. INTRODUCTION

Model Predictive Control (MPC) [1], [2] enables impressive performance on complex, agile robots [3]–[8]. However, its computational cost often limits the opportunities for onboard, real-time deployment [9], or takes away critical computational resources needed by other components governing the autonomous system. Recent works have mitigated MPC’s computational requirements by relying on computationally efficient deep neural network (DNN) policies that are trained to imitate task-relevant demonstrations generated by MPC in an offline training phase. Such demonstrations are generally collected via Imitation Learning (IL) [10]–[12], where the MPC acts as an expert that provides demonstrations, and the DNN policy is treated as a student, trained via supervised learning.

The authors are with the Department of Aeronautics and Astronautics, Massachusetts Institute of Technology. {atagliab, jhow}@mit.edu.

Work funded by the Air Force Office of Scientific Research MURI FA9550-19-1-0386.

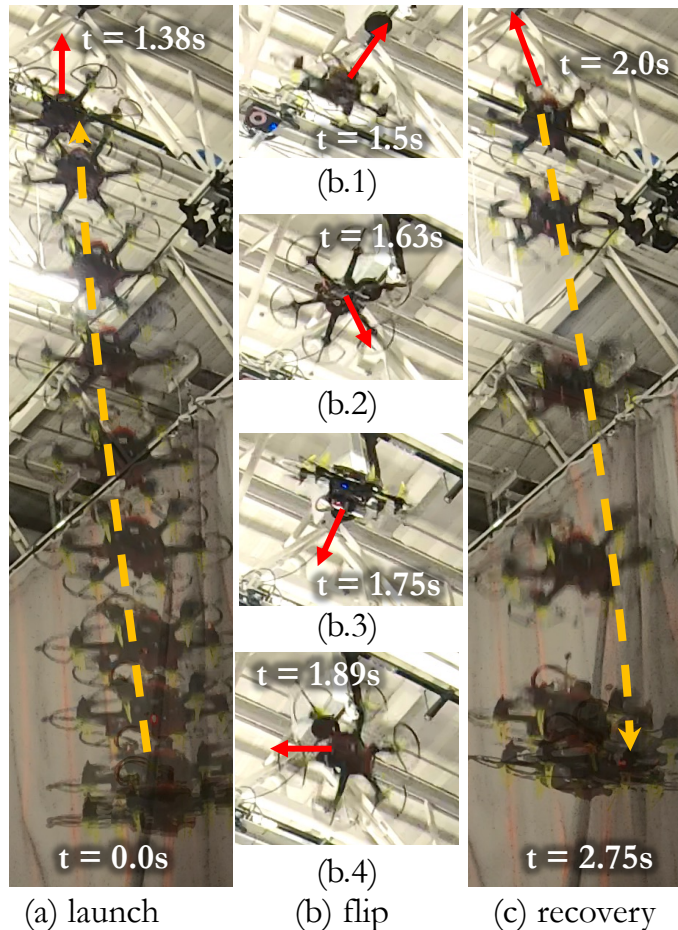


Fig. 1: Time-lapse figure showing an acrobatic maneuver (flip) performed by our multirotor, using a policy learned from a Robust Tube MPC variant that uses nonlinear models, and that is learned in a few minutes requiring only two demonstrations (one performing our proposed tube-guided data augmentation, and one for fine-tuning). (a) shows the robot accelerating upwards until it reaches the optimal altitude found by MPC. The red arrow denotes the directions of the thrust vector (aligned with the body z -axis), while the yellow arrow denotes the approximate trajectory. (b) shows the robot performing a 360° rotation around its body x -axis. This phase takes only about 0.5s. (c) shows the robot successfully decelerating until it reaches a vertical velocity < 1 m/s, followed by its landing. The learned policy runs onboard (Nvidia Jetson TX2, CPU) at 100Hz. This experiment demonstrates the ability of our approach to efficiently generate policies from MPC that can withstand real-world uncertainties and disturbances, even when leveraging models that operate in highly nonlinear regimes.

A common issue in existing IL methods (e.g., Behavior Cloning (BC) [13]–[15], Dataset-Aggregation (DAgger) [16]) is that they require to collect a relatively large number of MPC demonstrations, even for a single task like tracking a specific trajectory. This drawback introduces two significant challenges: firstly, it requires a substantial number of queries to the

computationally-expensive MPC expert, demanding expensive training equipment. Secondly, it leads to a considerable volume of queries to the training environment, which restricts data collection in computationally-expensive simulations (e.g., fluid-simulators) or requires numerous hours of real-time demonstrations on the physical robot, making it impractical.

One of the causes for such demonstration-inefficiency is the need to take into account and correct for the compounding of errors in the learned policy [16], which may otherwise create shifts (*covariate shifts*) from the training distribution, with catastrophic consequences [13]. These distribution shifts can be caused by: (a) approximation errors in the learned policy; (b) mismatches, e.g., due to modeling errors, between the simulator used to collect demonstrations and the deployment domain (i.e., sim2real gap); or (c) model changes or disturbances that may not be present in a controlled training environment (lab/factory when training on a real robot), but that do appear during deployment in the real-world (i.e., lab2real gap). Approaches employed to compensate for these *gaps* and generate a robust policy, such as Domain Randomization (DR) [17], [18], introduce additional challenges, such as the need to apply disturbances or model changes during training.

In this work, we address the problem of generating a robust DNN policy from MPC in a demonstration and computationally efficient manner by designing a computationally-efficient data augmentation (DA) strategy that systematically compensates for the effects of covariate shifts that might be encountered during real-world deployment. Our approach, depicted in Fig. 2, relies on a prior model of the perturbations/uncertainties encountered in a deployment domain, which is used to generate a robust version of the given MPC, called Robust Tube MPC (RTMPC), to collect demonstrations and to guide the DA strategy. The key idea behind this DA strategy consists in observing that the RTMPC framework provides: (a) information on the states that the robot may visit when subject to uncertainty. This is represented by a *tube* that contains the collected demonstration; the tube can be used to identify/generate extra relevant states for DA; and (b) an *ancillary controller* that maintains the robot inside the tube regardless of the realization of uncertainties; this controller can be used to generate extra actions.

This article extends our prior conference paper [19], where the focus was on efficiently generating robust trajectory tracking policies from a *linear* MPC. In this new work, we additionally provide a strategy to generate a DNN policy to reach a desired state using a *nonlinear* MPC expert, presenting a new methodology that can be used to perform DA in a computationally-efficient way. This extension is non-trivial, as the *ancillary controller* in the nonlinear RTMPC framework requires, unlike the linear case, expensive computations to generate extra actions for DA, resulting in long training times when performing DA. This new work (i) solves the computational-efficiency issues in the ancillary controller of nonlinear RTMPC by generating an approximation of the actions corresponding to extra state samples for DA. Additionally, this work presents (ii) a policy fine-tuning procedure to minimize the impact on performance introduced by our approximation; (iii) a formulation of nonlinear RTMPC for

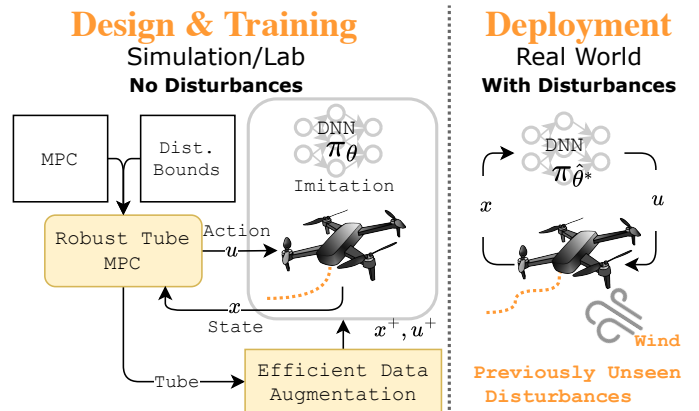


Fig. 2: Overview of the proposed approach to generate a DNN-based policy π_θ from a computationally expensive MPC in a demonstration and training-efficient way. We do so by generating a RTMPC using bounds of the disturbances encountered in the deployment domain. We use properties of the tube to derive a computationally efficient DA strategy that generates extra state-action pairs (x^+, u^+), obtaining $\pi_{\hat{\theta}^*}$ via IL. Our approach enables zero-shot transfer from a single demonstration collected in simulation (*sim2real*) or a controlled environment (lab, factory, *lab2real*).

acrobatic flights on multirotors; (iv) numerical comparison to IL baselines; (v) numerical comparison of different tube-sampling strategies; (vi) new real-world experiments with policies that leverage nonlinear models.

We tailor our approach to the task of efficiently learning robust policies for agile flight on a multirotor. First, we demonstrate in experiments trajectory tracking capabilities with a policy learned from a linear trajectory tracking RTMPC. The policy is learned from a *single* demonstration collected in simulation or directly on the real robot, and it is robust to previously-unseen wind disturbances. Second, we demonstrate the ability to generate a policy from a go-to-goal-state nonlinear RTMPC capable of performing acrobatic maneuvers, such as a 360 degrees flip. These maneuvers are performed under real-world uncertainties, using a policy obtained from only *two* demonstrations and in less than 100s of training time.

In summary, our work presents the following **contributions**:

- A procedure to *efficiently* learn *robust* policies from MPC. Our procedure is: 1) *demonstration-efficient*, as it requires a small number of queries to the training environment, resulting in a method that enables learning from a single MPC demonstration collected in simulation or on the real robot; 2) *training-efficient*, as it reduces the number of computationally expensive queries to the computationally expensive MPC expert using a computationally efficient DA strategy; 3) *generalizable*, as it produces policies robust to disturbances not experienced during training.
- We generalize the demonstration-efficient policy learning strategy proposed in our previous conference paper [19] with the ability to efficiently learn robust and generalizable policies from variants of MPC that use nonlinear models.
- Extensive simulations and comparisons with state-of-the-art IL methods and robustification strategies.
- Experimental evaluation on the challenging task of trajectory tracking and acrobatic maneuvers on a multirotor, presenting the first instance of sim2real transfer of a policy trained after a single demonstration, and robust to previously unseen real-world uncertainties.

II. RELATED WORKS

A. Explicit MPC.

A well-established method to generate a computationally efficient representation from linear MPC consists in *explicit* MPC [1]. This approach pre-computes offline a policy by partitioning the feasible state space in polytopic regions and by solving an optimal control problem for each region; the online optimization problem is reduced to finding the polytopic region corresponding to the current state via a look-up table. However, the memory requirement and computational complexity of explicit MPC grow exponentially in the number of constraints [1], [20]. Recent work has replaced look-up tables with DNNs [20]–[23], yielding to explicit MPC approximations that can be queried more efficiently. Although promising, these methods have been mainly studied in the context of linear systems, and do not leverage task-specific demonstrations to identify the more relevant parts of the feasible state space, therefore missing opportunities to optimize their performance or training efforts for those more relevant regions. Our work leverages task-relevant demonstrations and IL to focus the efforts of the policy learning procedure on the most relevant parts of the policy input space, while learning from MPC that use nonlinear models.

B. Policy Learning from MPC for Mobile Robot Control.

Learning policies from MPC is a strategy widely employed in the robotics literature to reduce the onboard computational cost of this type of controller. Close to our work, [10] learns to perform acrobatic maneuvers with a quadrotor from MPC using DAGger combined with DR, by collecting 150 demonstrations in simulation. Ref. [24] uses DAGger combined with an MPC based on differential dynamic programming (DDP) [25] for agile off-road autonomous driving using about 24 laps¹ around their racetrack for the first DAGger iteration. All these examples demonstrate the *performance* that can be achieved when imitation-learning policies from MPC, but they also highlight that current methods require a large number of interactions with the MPC expert and the training environment, resulting in longer training times or complex data collection procedures.

Methods based on Guided Policy Search (GPS) [26] use trajectories and samples from model-based trajectory planners, including MPC, to train DNN policies. For examples, GPS has been employed for navigation of a multirotor [27], [28], and to control a legged robot [12], [29]. These methods are in general more sample-efficient than IL strategies, thanks to the addition of guiding samples during policy training [26]. However, these methods do not *explicitly* account for model and environment uncertainties, resulting in policies with limited robustness. Ref. [27] for example, demonstrates in simulation robustness to up to 3.3% in weight perturbations of a multirotor, while our approach demonstrates robustness to perturbations up to 30%.

¹Obtained using Table 2 in [24], considering 6000 observation/action pairs sampled at 50 Hz while racing on a 30 m long racetrack with an average speed of 6 m/s.

C. Robustness in Imitation Learning

Robustness is a fundamental requirement for the real-world deployment of policies obtained via IL, as it is needed to compensate for the distribution shifts caused by the *sim2real* or *lab2real* (i.e., when collecting demonstrations on the real robot in a controlled environment and then deploying in the real world) transfers. Robustness to these types of *shifts* can be achieved by modifying the training domain so that its dynamics match the ones encountered in the deployment domain. This is done, for example, via DR [17], which applies random model errors/disturbances, sampled from a predefined set of possible perturbations, during data collection in simulation. Ref. [30], [31], instead, propose to match the training (source) and deployment (target) domain by estimating a model of the target domain from a few interactions with it. Although effective, these approaches require many demonstrations/interactions with the environment in order to take into account all the possible instantiations of model errors/disturbances that might be encountered in the target domain, limiting the opportunities for *lab2real* transfers, or increasing the data collection effort when training in simulation. An alternative avenue relies on modifying the actions of the expert to ensure that the state distribution visited at training time matches the one encountered at deployment time. DART [32] does so by applying to the actions of the expert some additive noise, sampled from a distribution designed to minimize the covariate shift between the source and target domain. Ref. [33], [34] propose instead to modify the expert actions so that the resulting transition function matches the transition that will be encountered in the target domain. These works have been designed in the context of learning from human demonstrations, therefore missing opportunities to exploit extra information available to the MPC to reduce the number of MPC/environment interactions.

D. Data Augmentation for Efficient/Robust Imitation Learning

A key idea in GPS [26] consists in generating extra state-action samples (guiding samples) from trajectory planners for improved sample efficiency in policy learning. Specifically, the authors leveraged an iterative linear quadratic regulator (ILQR) [5] expert to generate guiding samples around the optimal trajectory found by the controller. Similarly, the authors in [29] observe that adding extra states and actions sampled from the neighborhood of the optimal solution found by the ILQR expert can reduce the number of demonstrations required to learn a policy when using DAGger. These works highlight the benefits of DA when learning policies from model-based experts, but the expert demonstrations and the distribution of the samples they generate do not *explicitly* account for the effects of uncertainty, therefore producing policies that are not robust. Our work leverages a robust variant of MPC called RTMPC [35], [36], to provide robust demonstrations and a DA strategy that accounts for the effects of uncertainties. Specifically, the DA strategy is obtained by using an outer-approximation of the robust control invariant set (*tube*) as a support of the sampling distribution, ensuring that the guiding samples produce robust policies. This idea is related to the

recent LAG-ROS framework [37], which provides a learning-based method to compress a global planner in a DNN by extracting relevant information from the robust tube. LAG-ROS emphasizes the importance of nonlinear contraction-based controllers (e.g., CV-STEM [38]) to obtain robustness and stability guarantees. Our contribution emphasizes instead minimal requirements - namely a tube and an *efficient* DA strategy - to achieve demonstration-efficiency and robustness to real-world conditions. By decoupling these aspects from the need for complex control strategies, our work greatly simplifies the controller design. Additionally, different from LAG-ROS, the DA procedures presented in our work do not require solving a large optimization problem for every extra state-action sample generated (achieving computational efficiency during training) and can additionally leverage interactive experts (e.g., DAgger) to trade off the number of interactions with the environment with the number of extra samples from DA (further improving training efficiency).

Recent work [39], [40] exploited local approximations of the solutions found when solving the nonlinear program (NLP) associated with MPC to efficiently generate extra state-actions samples for DA in policy learning. Similar to our work, [39] uses a parametric sensitivity-based approximation of the solution to efficiently generate extra states and actions. Different from our work, however, their method proposes sampling of the entire feasible state space to learn a policy, while our work focuses instead on task-relevant demonstrations, a more computationally and data-efficient solution. The recently presented extension [40] solves this issue by leveraging interactive experts (e.g., DAgger). However, both [39], [40] do not *explicitly* account for the effects of uncertainties, neither in the design of the expert, nor in the way that extra states are generated, resulting in policies with limited robustness. Thanks to our robust expert, our approach not only accounts for uncertainties during demonstration collection and in the distribution of samples for DA, but it can additionally account for the errors introduced in the DA procedure by further constraint tightening and updating the tube size. Additionally, thanks to the strong prior on the state distribution under uncertainty produced by the tube in RTMPC, our DA strategy can quickly cover the task-relevant parts of the state space, obtaining demonstration-efficiency. Last, unlike prior work, we experimentally validate our approach, demonstrating it on a system whose models has a large state size (state size 8 and 10), whereas previous work focuses on lower-dimensional systems (state size 2) and only in simulation.

III. PROBLEM STATEMENT

This part describes the problem of learning a robust policy in a demonstration and computationally efficient way by imitating an MPC expert demonstrator. Robustness and efficiency are determined by the ability to design an IL procedure that can compensate for the covariate shifts induced by uncertainties encountered during real-world deployment while collecting demonstrations in a domain (the training domain) that presents only a subset of those uncertainty realizations. Our problem statement follows the one of robust IL (e.g., DART [32]),

modified to use deterministic policies/experts and to account for the differences in uncertainties encountered in deployment and training domains. Additionally, we present a common approach employed to address the covariate shift issues caused by uncertainties, DR, highlighting its limitations.

A. Assumptions and Notation

System Dynamics. We assume the dynamics of the real system are Markovian and stochastic [41], and can be described by a twice continuously differentiable function $f(\cdot)$:

$$\mathbf{x}_{t+1} = f(\mathbf{x}_t, \mathbf{u}_t) + \mathbf{w}_t, \quad (1)$$

where $\mathbf{x}_t \in \mathbb{X} \subseteq \mathbb{R}^{n_x}$ represents the state, $\mathbf{u}_t \in \mathbb{U} \subseteq \mathbb{R}^{n_u}$ the control input in the compact subsets \mathbb{X} , \mathbb{U} . $\mathbf{w}_t \in \mathbb{W}_{\mathcal{D}} \subseteq \mathbb{R}^{n_x}$ is an unknown state perturbation, belonging to a compact convex set $\mathbb{W}_{\mathcal{D}}$ containing the origin. Stochasticity in Eq. (1) is introduced by \mathbf{w}_t , sampled from $\mathbb{W}_{\mathcal{D}}$ under a (possibly unknown) probability distribution, capturing the effects of noise, approximation errors in the learned policy, model changes, and other disturbances acting on the system during training or under real-world conditions at deployment.

Sim2Real and Lab2Real Transfer Setup. Two different domains \mathcal{D} are considered: a training domain \mathcal{S} (*source*) and a deployment domain \mathcal{T} (*target*). The two domains differ in their transition probabilities, and we assume that $\mathbb{W}_{\mathcal{S}} \subset \mathbb{W}_{\mathcal{T}}$, representing the fact that training is usually performed in simulation or in a controlled/lab environment under some nominal model errors/disturbances ($\mathbf{w} \in \mathbb{W}_{\mathcal{S}}$), while at deployment a larger set of perturbations ($\mathbf{w} \in \mathbb{W}_{\mathcal{T}}$) can be encountered.

MPC Expert. We assume that we are given an MPC expert demonstrator that plans along a $N + 1$ -steps horizon. The expert is given the current state \mathbf{x}_t , and $\mathbf{X}_t^{\text{des}} \in \mathbb{X}_M^{\text{des}} := \{\mathbb{X}\}_{i=0}^M$, representing a desired state to be reached ($M = 0$), or a state trajectory to be followed ($M = N + 1$). Then, the MPC expert generates control actions by solving an Optimal Control (OC) problem of the form:

$$\begin{aligned} \bar{\mathbf{X}}_t^*, \bar{\mathbf{U}}_t^* \in \underset{\bar{\mathbf{x}}_t, \bar{\mathbf{u}}_t}{\text{argmin}} & J_{N,M}(\bar{\mathbf{X}}_t, \bar{\mathbf{U}}_t, \mathbf{X}_t^{\text{des}}) \\ \text{subject to} & \bar{\mathbf{x}}_{0|t} = \mathbf{x}_t, \\ & \bar{\mathbf{x}}_{i+1|t} = f(\bar{\mathbf{x}}_{i|t}, \bar{\mathbf{u}}_{i|t}), \\ & \bar{\mathbf{x}}_{i|t} \in \mathbb{X}, \bar{\mathbf{u}}_{i|t} \in \mathbb{U}, \\ & i = 0, \dots, N - 1. \end{aligned} \quad (2)$$

where $J_{N,M}$ represents the cost to be minimized (where N denotes the dependency on the planning horizon, and M on the type of task, i.e., tracking or reaching a goal state), and $\bar{\mathbf{X}}_t = \{\bar{\mathbf{x}}_{0|t}, \dots, \bar{\mathbf{x}}_{N|t}\}$ and $\bar{\mathbf{U}}_t = \{\bar{\mathbf{u}}_{0|t}, \dots, \bar{\mathbf{u}}_{N-1|t}\}$ are sequences of states and actions along the planning horizon, where the notation $\bar{\mathbf{x}}_{i|t}$ indicates the planned state at the future time $t + i$, as planned at the current time t . At every timestep t , given \mathbf{x}_t , the control input applied to the real system is the first element of $\bar{\mathbf{U}}_t^*$, resulting in an implicit deterministic control law (policy) that we denote as $\pi_{\theta^*} : \mathbb{X} \times \mathbb{X}_M^{\text{des}} \rightarrow \mathbb{U}$.

DNN Student Policy. As for the MPC expert, we model the DNN student policy as a deterministic policy π_{θ} , with

parameters θ . When considering trajectory tracking tasks, the policy takes as input the current state and the desired reference trajectory segment, $\pi_\theta : \mathbb{X} \times \mathbb{X}_{N+1}^{\text{des}} \rightarrow \mathbb{U}$. When considering the task of reaching a goal state, the policy takes as input the current state, the desired goal state and the current timestep $t \in \mathbb{I}_{>0}$, $\pi_\theta : \mathbb{X} \times \mathbb{X}_0^{\text{des}} \times \mathbb{I}_{>0} \rightarrow \mathbb{U}$.

Transition Probabilities. We denote the state transition probability under π_θ in a domain \mathcal{D} for a given goal-reaching or trajectory tracking task as $p_{\pi_\theta, \mathcal{D}}(\mathbf{x}_{t+1} | \mathbf{x}_t)$. We highlight that the probability of collecting a T -step trajectory $\xi = \{\mathbf{x}_0, \mathbf{u}_0, \mathbf{x}_1, \mathbf{u}_1, \dots, \mathbf{x}_T\}$, given a policy π_θ , depends on the deployment environment \mathcal{D} :

$$p(\xi | \pi_\theta, \mathcal{D}) = p(\mathbf{x}_0) \prod_{t=0}^{T-1} p_{\pi_\theta, \mathcal{D}}(\mathbf{x}_{t+1} | \mathbf{x}_t), \quad (3)$$

where $p(\mathbf{x}_0)$ represents the initial state distribution.

B. Robust Imitation Learning Objective

The objective of robust IL, following [32], is to find parameters θ of π_θ that minimize a distance metric $\mathcal{L}(\theta, \theta^* | \xi)$ from the MPC expert π_{θ^*} . This metric captures the differences between the actions generated by the expert π_{θ^*} and the action produced by the student π_θ across the distribution of trajectories induced by the student policy π_θ , in the perturbed domain \mathcal{T} :

$$\hat{\theta}^* = \arg \min_{\theta} \mathbb{E}_{p(\xi | \pi_\theta, \mathcal{T})} \mathcal{L}(\theta, \theta^* | \xi). \quad (4)$$

The distance metric considered in this work is the Mean Squared Error (MSE) loss:

$$\mathcal{L}(\theta, \theta^* | \xi) = \frac{1}{T} \sum_{t=0}^{T-1} \|\pi_\theta(\mathbf{x}_t^{\text{in}}) - \pi_{\theta^*}(\mathbf{x}_t, \mathbf{X}_t^{\text{des}})\|_2^2. \quad (5)$$

where $\mathbf{x}_t^{\text{in}} = \{\mathbf{x}_t, \mathbf{X}_t^{\text{des}}\}$ for trajectory tracking tasks, and $\mathbf{x}_t^{\text{in}} = \{\mathbf{x}_t, \mathbf{X}_t^{\text{des}}, t\}$ for go-to-goal-state tasks.

Covariate Shift due to Sim2real and Lab2real Transfer. Because in practice we do not have access to the target environment, the goal of Robust IL is to try to solve Eq. (4) by finding an approximation of the optimal policy parameters $\hat{\theta}^*$ using data from the source environment:

$$\hat{\theta}^* = \arg \min_{\theta} \mathbb{E}_{p(\xi | \pi_\theta, \mathcal{S})} \mathcal{L}(\theta, \theta^* | \xi). \quad (6)$$

The way this minimization is solved depends on the chosen IL algorithm. The performance of the learned policy in the target and source domains can be related via:

$$\begin{aligned} \mathbb{E}_{p(\xi | \pi_\theta, \mathcal{T})} \mathcal{L}(\theta, \theta^* | \xi) &= \\ & \underbrace{\mathbb{E}_{p(\xi | \pi_\theta, \mathcal{T})} \mathcal{L}(\theta, \theta^* | \xi) - \mathbb{E}_{p(\xi | \pi_\theta, \mathcal{S})} \mathcal{L}(\theta, \theta^* | \xi)}_{\text{covariate shift due to transfer}} \\ & \quad + \underbrace{\mathbb{E}_{p(\xi | \pi_\theta, \mathcal{S})} \mathcal{L}(\theta, \theta^* | \xi)}_{\text{IL objective}}, \end{aligned} \quad (7)$$

which clearly shows the presence of a covariate shift induced by the transfer. The last term corresponds to the objective minimized by performing IL in \mathcal{S} . Attempting to solve Eq. (4) by directly optimizing Eq. (6) (e.g., via BC [13]) offers no assurances of finding a policy with good performance in \mathcal{T} .

C. Compensating Transfer Covariate Shifts via Domain Randomization.

A well-known strategy to compensate for the effects of covariate shifts between source and target domain is DR [17], which modifies the transition probabilities of the source \mathcal{S} by trying to ensure that the trajectory distribution in the modified training domain \mathcal{S}_{DR} matches the one encountered in the target domain: $p(\xi | \pi_\theta, \mathcal{S}_{\text{DR}}) \approx p(\xi | \pi_\theta, \mathcal{T})$. This is done by applying perturbations to the robot during demonstration collection, sampling perturbations $\mathbf{w} \in \mathbb{W}_{\text{DR}}$ according to some knowledge/hypotheses on their distribution $p_{\mathcal{T}}(\mathbf{w})$ in the target domain [17], obtaining the perturbed trajectory distribution $p(\xi | \pi_\theta, \mathcal{S}, \mathbf{w})$. The minimization of Eq. (4) can then be approximately performed by minimizing instead:

$$\mathbb{E}_{p_{\mathcal{T}}(\mathbf{w})} [\mathbb{E}_{p(\xi | \pi_\theta, \mathcal{S}, \mathbf{w})} \mathcal{L}(\theta, \theta^* | \xi)]. \quad (8)$$

This approach, however, requires the ability to apply disturbances/model changes to the system, which may be unpractical e.g., in the *lab2real* setting, and may require a large number of demonstrations due to the need to sample enough state perturbations \mathbf{w} .

IV. EFFICIENT LEARNING FROM LINEAR RTMPC

In this Section, we present the strategy to efficiently learn robust policies from MPC when the system dynamics in Eq. (1) can be well approximated by a linear model of the form:

$$\mathbf{x}_{t+1} = \mathbf{A} \mathbf{x}_t + \mathbf{B} \mathbf{u}_t + \mathbf{w}_t. \quad (9)$$

First, we present the Robust Tube variant of linear MPC, RTMPC, that we employ to collect demonstrations (Section IV-A). Then, we present a strategy that leverages information available from the RTMPC expert to compensate for the covariate shifts caused by uncertainties and mismatches between the training and deployment domains (Section IV-B). Our strategy is based on a DA procedure that can be combined with different IL methods (on-policy, such as DAgger [16], and off-policy, such as BC, [13]) for improved efficiency/robustness in the policy learning procedure. The RTMPC expert is based on [35] but with the objective function modified to track desired trajectories, as trajectory-tracking tasks will be the focus of the experimental evaluation of policies learned from this controller (Section VII).

A. Trajectory Tracking RTMPC Expert Formulation

RTMPC is a type of robust MPC that regulates the system in Eq. (9) while ensuring satisfaction of the state and actuation constraints \mathbb{X}, \mathbb{U} regardless of the disturbances $\mathbf{w} \in \mathbb{W}_{\mathcal{T}}$.

Mathematical Preliminaries. Let $\mathbb{A} \subset \mathbb{R}^n$ and $\mathbb{B} \subset \mathbb{R}^n$ be convex polytopes, and let $\mathbb{C} \in \mathbb{R}^{m \times n}$ be a linear mapping. In this context, we establish the following definition:

- a) Linear mapping: $\mathbb{C}\mathbb{A} := \{\mathbf{C}\mathbf{a} \in \mathbb{R}^m \mid \mathbf{a} \in \mathbb{A}\}$
- b) Minkowski sum: $\mathbb{A} \oplus \mathbb{B} := \{\mathbf{a} + \mathbf{b} \in \mathbb{R}^n \mid \mathbf{a} \in \mathbb{A}, \mathbf{b} \in \mathbb{B}\}$
- c) Pontryagin diff.: $\mathbb{A} \ominus \mathbb{B} := \{\mathbf{c} \in \mathbb{R}^n \mid \mathbf{c} + \mathbf{b} \in \mathbb{A}, \forall \mathbf{b} \in \mathbb{B}\}$.

Optimization Problem. At each time step t , trajectory tracking RTMPC receives the current robot state \mathbf{x}_t and a desired trajectory $\mathbf{X}_t^{\text{des}} = \{\mathbf{x}_{0|t}^{\text{des}}, \dots, \mathbf{x}_{N|t}^{\text{des}}\}$ spanning $N + 1$ steps as

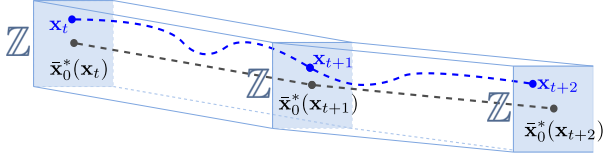


Fig. 3: Illustration of the robust control invariant tube \mathbb{Z} centered around the optimal reference $\bar{\mathbf{x}}_0^*(\mathbf{x}_t)$ computed by RTMPC at every state \mathbf{x} , for a system with state dimension $n_x = 2$.

input. It then computes a sequence of reference (“safe”) states $\bar{\mathbf{X}}_t = \{\bar{\mathbf{x}}_{0|t}, \dots, \bar{\mathbf{x}}_{N|t}\}$ and actions $\bar{\mathbf{U}}_t = \{\bar{\mathbf{u}}_{0|t}, \dots, \bar{\mathbf{u}}_{N-1|t}\}$ that ensure constraint compliance regardless of the realization of $\mathbf{w}_t \in \mathbb{W}_{\mathcal{T}}$. This is achieved by solving the following optimization problem:

$$\begin{aligned} \bar{\mathbf{U}}_t^*, \bar{\mathbf{X}}_t^* &= \underset{\bar{\mathbf{U}}_t, \bar{\mathbf{X}}_t}{\operatorname{argmin}} \|\mathbf{e}_{N|t}\|_{\mathbf{P}_x}^2 + \sum_{i=0}^{N-1} \|\mathbf{e}_{i|t}\|_{\mathbf{Q}_x}^2 + \|\mathbf{u}_{i|t}\|_{\mathbf{R}_u}^2 \\ &\text{subject to } \bar{\mathbf{x}}_{i+1|t} = \mathbf{A}\bar{\mathbf{x}}_{i|t} + \mathbf{B}\bar{\mathbf{u}}_{i|t}, \\ &\bar{\mathbf{x}}_{i|t} \in \mathbb{X} \ominus \mathbb{Z}, \quad \bar{\mathbf{u}}_{i|t} \in \mathbb{U} \ominus \mathbf{K}\mathbb{Z}, \\ &\mathbf{x}_t \in \mathbb{Z} \oplus \bar{\mathbf{x}}_{0|t}, \quad i = 0, \dots, N-1 \end{aligned} \quad (10)$$

where $\mathbf{e}_{i|t} = \bar{\mathbf{x}}_{i|t} - \mathbf{x}_{i|t}^{\text{des}}$ is the tracking error. The positive definite matrices \mathbf{Q}_x , \mathbf{R}_u define the trade-off between deviations from the desired trajectory and actuation usage, while $\|\mathbf{e}_{N|t}\|_{\mathbf{P}_x}^2$ is the terminal cost. \mathbf{P}_x and \mathbf{K} are obtained by formulating an infinite horizon optimal control LQR problem using \mathbf{A} , \mathbf{B} , \mathbf{Q}_x and \mathbf{R}_u and by solving the associated algebraic Riccati equation [42]. To achieve recursive feasibility, we ensure a sufficiently long prediction horizon is selected, as commonly practiced [43], while omitting the inclusion of terminal set constraints.

Tube and Ancillary Controller. A control input for the real system is generated by RTMPC via an *ancillary controller*:

$$\mathbf{u}_t = \bar{\mathbf{u}}_t^* + \mathbf{K}(\mathbf{x}_t - \bar{\mathbf{x}}_t^*), \quad (11)$$

where $\bar{\mathbf{u}}_t^* = \bar{\mathbf{u}}_{0|t}^*$ and $\bar{\mathbf{x}}_t^* = \bar{\mathbf{x}}_{0|t}^*$. As shown in Fig. 3, this controller ensures that the system remains inside a *tube* (with “cross-section” \mathbb{Z}) centered around $\bar{\mathbf{x}}_t^*$ regardless of the realization of the disturbances in $\mathbb{W}_{\mathcal{T}}$, provided that the tube contains the initial state of the system (constraint $\mathbf{x}_t \in \mathbb{Z} \oplus \bar{\mathbf{x}}_{0|t}$). The set \mathbb{Z} is a disturbance invariant set for the closed-loop system $\mathbf{A}_K := \mathbf{A} + \mathbf{B}\mathbf{K}$, satisfying the property that $\forall \mathbf{x}_j \in \mathbb{Z}$, $\forall \mathbf{w}_j \in \mathbb{W}_{\mathcal{T}}$, $\forall j \in \mathbb{N}^+$, $\mathbf{x}_{j+1} = \mathbf{A}_K \mathbf{x}_j + \mathbf{w}_j \in \mathbb{Z}$ [35]. \mathbb{Z} can be computed offline using \mathbf{A}_K and the model of the disturbance \mathbb{W} via ad-hoc analytic algorithms [1], [35], or can be learned from data [44].

B. Covariate Shift Compensation via Sampling Augmentation

We observe that training a policy by collecting demonstrations in a controlled source domain \mathcal{S} , with the objective of deploying it in the target domain \mathcal{T} , may introduce a sample selection bias [45], i.e., demonstrations are collected only around the nominal state distribution, and not around the distribution induced by perturbations encountered in the *sim2real* and *lab2real* transfer. Such selection bias is a known

cause of distribution shifts [45], and it is usually mitigated by re-weighting collected samples in a way that takes into account their likelihood of appearing in the target domain \mathcal{T} (e.g., via importance-sampling). These approaches, however, do not apply in our case, since we do not have access to samples/demonstrations collected in \mathcal{T} .

In this work, we propose to mitigate the covariate shift introduced by the policy generation procedure not only by collecting demonstrations from the RTMPC but by using additional information computed in the controller. Specifically, during the collection of a trajectory ξ in the source domain \mathcal{S} , we utilize instead the tube computed by the RTMPC demonstrator to obtain knowledge of the states that the system may visit when subjected to perturbations. Given this information, we propose a tube-guided DA strategy, called Sampling Augmentation (SA), that samples states from the tube. The corresponding actions are provided at low computational cost by the ancillary controller of the RTMPC expert. The collected state-actions pairs are then included in the dataset of demonstrations used to train a policy. The following paragraphs frame the tube sampling problem in the context of covariate shift reduction in IL, and discuss tube-sampling strategies.

Tube as a Model of State Distribution Under Uncertainties.

The key intuition of the proposed approach is the following. We observe that, although the density $p(\xi|\pi_{\theta}, \mathcal{T})$ is unknown, an approximation of its support \mathfrak{R} , given a demonstration ξ collected in the source domain \mathcal{S} , is known. Such support corresponds to the tube computed by the RTMPC when collecting ξ :

$$\mathfrak{R}_{\xi^+|\pi_{\theta^*}, \xi} = \bigcup_{t=0}^{T-1} \{\bar{\mathbf{x}}_t^* \oplus \mathbb{Z}\}. \quad (12)$$

where ξ^+ is a trajectory in the tube of ξ . This is true thanks to the ancillary controller in Eq. (11), which ensures that the system remains inside Eq. (12) for every possible realization of $\mathbf{w} \in \mathbb{W}_{\mathcal{T}}$. The ancillary controller additionally provides a computationally efficient way to obtain the actions to apply for every state inside the tube. Let $\mathbf{x}_{t,j}^+ \in \bar{\mathbf{x}}_t^* \oplus \mathbb{Z}$, i.e., $\mathbf{x}_{t,j}^+$ is a state inside the tube computed when the system is at \mathbf{x}_t , then the corresponding robust control action $\mathbf{u}_{t,j}^+$ is:

$$\mathbf{u}_{t,j}^+ = \bar{\mathbf{u}}_t^* + \mathbf{K}(\mathbf{x}_{t,j}^+ - \bar{\mathbf{x}}_t^*). \quad (13)$$

For every timestep t in ξ , extra state-action samples $(\mathbf{x}_{t,j}^+, \mathbf{u}_{t,j}^+)$, with $j = 1, \dots, N_s$ collected from within the tube can be used to augment the dataset employed to train the policy, obtaining a way to approximate the expected risk in the domain \mathcal{T} by only having access to demonstrations collected in \mathcal{S} :

$$\begin{aligned} \mathbb{E}_{p(\xi|\pi_{\theta}, \mathcal{T})} \mathcal{L}(\theta, \theta^*|\xi) &\approx \\ \mathbb{E}_{p(\xi|\pi_{\theta}, \mathcal{S})} [\mathcal{L}(\theta, \theta^*|\xi) + \mathbb{E}_{p(\xi^+|\pi_{\theta^*}, \xi)} \mathcal{L}(\theta, \theta^*|\xi^+)]. \end{aligned} \quad (14)$$

The demonstrations in the source domain \mathcal{S} can be collected using existing IL techniques, such as BC or DAgger.

Tube Approximation and Sampling Strategies. In practice, the density $p(\xi^+|\xi, \pi_{\theta^*})$ may not be available, making it difficult to establish which states to sample for DA. We consider an adversarial approach to the problem by sampling states that may be visited under worst-case perturbations. To efficiently

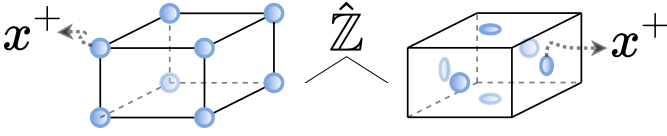


Fig. 4: The possible strategies to sample extra state-action pairs from an axis-aligned bounding box approximation of the tube of the RTMPC expert: dense (left) and sparse (right). The tube is represented for a system with state dimension $n_x = 3$.

compute those samples, we (outer) approximate the tube \mathbb{Z} with an axis-aligned bounding box $\hat{\mathbb{Z}}$. We investigate two strategies, shown in Fig. 4, to obtain state samples $\mathbf{x}_{t,j}^+$ at every state \mathbf{x}_t in ξ : i) dense sampling: sample extra states from the vertices of $\bar{\mathbf{x}}_t^* \oplus \hat{\mathbb{Z}}$. The approach produces $N_s = 2^{n_x}$ extra state-action samples. It is more conservative, as it produces more samples, but more computationally expensive. ii) sparse sampling: sample one extra state from the center of each *facet* of $\bar{\mathbf{x}}_t^* \oplus \hat{\mathbb{Z}}$, producing $N_s = 2n_x$ additional state-action pairs. It is less conservative and more computationally efficient.

V. EFFICIENT LEARNING FROM NONLINEAR RTMPC

In this Section, we design an IL and DA strategy, which is an extension of the one presented in Section IV, that enables robust and efficient policy learning from an MPC that employs nonlinear models of the form in Eq. (1). Different from Section IV, the focus here is on obtaining policies capable of reaching a desired goal state, as this will enable acrobatic maneuvers – the scenario considered in the evaluation of policies learned from this controller (Section VIII). To accomplish this, first, we use a nonlinear version of RTMPC, based on [36], to collect demonstrations that account for the effects of uncertainties. This expert is summarized in Section V-A. Second, we develop a computationally efficient tube-guided DA strategy leveraging the ancillary controller of the nonlinear RTMPC expert. Unfortunately, unlike in the linear RTMPC case, nonlinear RTMPC [36] uses Nonlinear Model Predictive Control (NMPC) as an ancillary controller. This limits the computational efficiency in DA, as the generation of extra state-action samples requires solving a large NLP associated with the ancillary NMPC (discussed in Section V-B). We overcome this issue by presenting, in Section V-C, a time-varying linear feedback law, approximation of the ancillary NMPC, that enables efficient generation of the extra data. This is done by leveraging the sensitivity of the control input to perturbations in the states visited during an initial demonstration collection procedure. Finally, in Section V-D, we address the approximation errors introduced by the sensitivity-based DA by presenting strategies to mitigate the gap, in performance and robustness, between the learned policy and the MPC expert.

A. Nonlinear RTMPC Expert Formulation

Nonlinear RTMPC [36] ensures state and actuation constraint satisfaction while controlling a nonlinear, uncertain system of the form in Eq. (1). This controller operates by solving two Optimal Control Problems (OCPs), one to compute a nominal safe plan, and one to track the safe plan (ancillary NMPC). **Nominal Safe Planner.** The first OCP, given an $N + 1$ -steps planning horizon, generates nominal safe state and

action open-loop plans $\mathbf{Z}_{t_0} = \{\mathbf{z}_{0|t_0}, \dots, \mathbf{z}_{N|t_0}\}$, $\mathbf{V}_{t_0} = \{\mathbf{v}_{0|t_0}, \dots, \mathbf{v}_{N-1|t_0}\}$. The plans are open-loop because they are generated only at time t_0 when the desired state and action pair $\mathbf{X}_{t_0}^{\text{des}} = \{\mathbf{x}_{t_0}^e, \mathbf{u}_{t_0}^e\}$, equilibrium pair for the nominal system, changes. The nominal safe plan is obtained from:

$$\begin{aligned} \mathbf{V}_{t_0}^*, \mathbf{Z}_{t_0}^* &= \underset{\mathbf{V}_{t_0}, \mathbf{Z}_{t_0}}{\operatorname{argmin}} J_{\text{RTMPC}}(\mathbf{Z}_{t_0}, \mathbf{V}_{t_0}, \mathbf{X}_{t_0}^{\text{des}}) \\ &\text{subject to } \mathbf{z}_{i+1|t_0} = f(\mathbf{z}_{i|t_0}, \mathbf{v}_{i|t_0}), \\ &\mathbf{z}_{i|t_0} \in \bar{\mathbb{Z}}, \mathbf{v}_{i|t_0} \in \bar{\mathbb{V}}, \\ &\mathbf{z}_{0|t_0} = \mathbf{x}_{t_0}, \mathbf{z}_{N|t_0} = \mathbf{x}_{t_0}^e. \end{aligned} \quad (15)$$

$J_{\text{RTMPC}} = \sum_{i=0}^{N-1} \|\mathbf{z}_{i|t_0} - \mathbf{x}_{t_0}^e\|_{\mathbf{Q}_z}^2 + \|\mathbf{v}_{i|t_0} - \mathbf{u}_{t_0}^e\|_{\mathbf{R}_v}^2$, where $\mathbf{Q}_z, \mathbf{R}_v$ are positive definite. A key idea in this approach involves imposing modified state and actuation constraints $\bar{\mathbb{Z}} \subset \mathbb{X}$ and $\bar{\mathbb{V}} \subset \mathbb{U}$ so that the generated nominal safe plan is at a specific distance from state and actuation constraints. To be more precise, similar to the linear RTMPC case (Eq. (10)), the given state constraints \mathbb{X} and actuation constraints \mathbb{U} are tightened (made more conservative) by an amount that accounts for the spread of trajectories induced by the ancillary controller when the system is subject to uncertainties, obtaining $\bar{\mathbb{Z}} \subset \mathbb{X}$ and $\bar{\mathbb{V}} \subset \mathbb{U}$. Different from the linear case, however, analytically computing the tightened constraints is challenging. Fortunately, as highlighted in [36], accurately computing these sets is not needed, and an outer approximation is sufficient. This approximation can be obtained via Monte-Carlo simulations [36] of the system under disturbances, or learned [44].

Ancillary NMPC. The second OCP corresponds to a trajectory tracking NMPC, that acts as an ancillary controller, to maintain the state of the uncertain system close to the reference generated by Eq. (15). The OCP is:

$$\begin{aligned} \bar{\mathbf{U}}_t^*, \bar{\mathbf{X}}_t^* &= \underset{\bar{\mathbf{U}}_t, \bar{\mathbf{X}}_t}{\operatorname{argmin}} \|\mathbf{e}_{N|t}\|_{\mathbf{P}_x}^2 + \sum_{i=0}^{N-1} \|\mathbf{e}_{i|t}\|_{\mathbf{Q}_x}^2 + \|\bar{\mathbf{u}}_{i|t} - \mathbf{v}_{i+t|t_0}^*\|_{\mathbf{R}_u}^2 \\ &\text{subject to } \bar{\mathbf{x}}_{i+1|t} = f(\bar{\mathbf{x}}_{i|t}, \bar{\mathbf{u}}_{i|t}) \\ &\bar{\mathbf{x}}_{0|t} = \mathbf{x}_t, \bar{\mathbf{u}}_{i|t} \in \bar{\mathbb{U}} \end{aligned} \quad (16)$$

where $\mathbf{e}_{i|t} = \bar{\mathbf{x}}_{i|t} - \mathbf{z}_{i+t-t_0|t_0}^*$ is the state tracking error. The positive definite matrices \mathbf{Q}_x and \mathbf{R}_u are tuning parameters and can differ from the ones in Eq. (15), while \mathbf{P}_x defines a terminal cost. Eq. (16) is solved at each timestep using the current state \mathbf{x}_t , while the action applied to the robot is $\mathbf{u}_t = \bar{\mathbf{u}}_{0|t}^*$. We note that the ancillary NMPC can have different tuning parameters than Eq. (15), including the discretization time of the dynamics and the prediction horizon N , providing additional degrees of freedom to shape the response of the system under uncertainties.

A key result of the employed nonlinear RTMPC [36] is that the ancillary NMPC in Eq. (16) maintains the trajectories of the uncertain system in Eq. (1) inside state and action tubes $\mathbb{T}^{\text{state}} \subset \mathbb{R}^{n_x}, \mathbb{T}^{\text{action}} \subset \mathbb{R}^{n_u}$ that contain the current nominal safe state and action trajectories $\mathbf{z}_{t|t_0}^*, \mathbf{v}_{t|t_0}^*$ from the OCP in Eq. (15). The state and action tubes are used to obtain the tightened state and actuation constraints $\bar{\mathbb{Z}}, \bar{\mathbb{V}}$, ensuring constraint satisfaction.

B. Solving the Ancillary NMPC

A large portion of the computational cost of deploying or collecting demonstrations from nonlinear RTMPC comes from the need to solve the OCP of the ancillary NMPC (Eq. (16)) at each timestep. In contrast, the OCP of the nominal safe plan (Eq. (15)) can be solved once per task (e.g., whenever the desired goal state $\mathbf{X}_{t_0}^{\text{des}}$ changes).

A state-of-the-art method to solve the OCP in Eq. (16) that yields high-quality solutions is Multiple Shooting [2]. In this approach, an OCP, discretized over a time grid, is transformed in a NLP that tries to find an optimal sequence of states and actions. This is done by forward-simulating the nonlinear dynamics on each interval (e.g., via an implicit Runge-Kutta (RK) integrator) while imposing additional continuity conditions. The resulting NLP can be solved via a sequential quadratic program (SQP), i.e., by repeatedly: i) linearizing the NLP around a given linearization point; ii) generating and solving a corresponding quadratic program (QP), obtaining a refined linearization point for the next SQP iteration. While capable of producing high-quality solutions, SQP methods incur large computational requirements due to the need of performing computationally-expensive system linearization and solving the associated QP one or more times per timestep.

C. Computationally-Efficient Data Augmentation using the Parametric Sensitivities

The tube $\mathbb{T}^{\text{state}}$ induced by the ancillary controller in Eq. (16) can be used to identify relevant regions of the state space for DA, as it approximates the support of the state distribution under uncertainties, as discussed in Section IV-B. However, generating the corresponding extra action samples using Eq. (16) can be very computationally inefficient, as it requires solving the associated SQP for every extra state sample, making DA computationally impractical, and defeating our initial objective of designing *computationally efficient* DA strategies.

In this work, we extend our efficient DA strategy, Sampling Augmentation (SA), to efficiently learn policies from nonlinear RTMPC by proposing instead to employ a time-varying, linear approximation of the ancillary NMPC – enabling efficient generation of extra state-action samples. Specifically, we observe that Eq. (16) solves the implicit feedback law:

$$\mathbf{u}_t = \bar{\mathbf{u}}_{0|t}^*(\boldsymbol{\chi}_t) := \kappa(\boldsymbol{\chi}_t), \quad \boldsymbol{\chi}_t := \{\mathbf{x}_t, t; \mathbf{V}_{t_0}^*, \mathbf{Z}_{t_0}^*\} \quad (17)$$

where we have denoted the current inputs $\boldsymbol{\chi}_t$ for convenience. Then, for each timestep of the trajectory collected during a demonstration in the source environment \mathcal{S} , with current ancillary NMPC input $\tilde{\boldsymbol{\chi}}_t = \{\tilde{\mathbf{x}}_t, \tilde{t}; \mathbf{V}_{t_0}^*, \mathbf{Z}_{t_0}^*\}$, we generate a local linear approximation of Eq. (17) by computing the first-order sensitivity of \mathbf{u}_t to the initial state \mathbf{x}_t :

$$\mathbf{K}_{\tilde{\boldsymbol{\chi}}_t} := \frac{\partial \bar{\mathbf{u}}_{0|t}^*}{\partial \mathbf{x}_t} \Big|_{\mathbf{x}_t = \tilde{\mathbf{x}}_t} = \left[\frac{\partial \bar{\mathbf{u}}_{0|t}^*}{\partial [\mathbf{x}_t]_1} \Big|_{\tilde{\mathbf{x}}_t}, \dots, \frac{\partial \bar{\mathbf{u}}_{0|t}^*}{\partial [\mathbf{x}_t]_{n_x}} \Big|_{\tilde{\mathbf{x}}_t} \right]. \quad (18)$$

The sensitivity matrix $\mathbf{K}_{\tilde{\boldsymbol{\chi}}_t} \in \mathbb{R}^{n_u \times n_x}$, enables us to compute extra actions $\mathbf{u}_{t,j}^+$ from states $\mathbf{x}_{t,j}^+ \in \mathbb{T}^{\text{state}}$, with $j = 1, \dots, N_s$, sampled from the tube:

$$\mathbf{u}_{t,j}^+ = \bar{\mathbf{u}}_{0|t}^* + \mathbf{K}_{\tilde{\boldsymbol{\chi}}_t}(\mathbf{x}_{t,j}^+ - \bar{\mathbf{x}}_{0|t}) := \hat{\kappa}(\mathbf{x}_{t,j}^+, \tilde{\boldsymbol{\chi}}_t). \quad (19)$$

The DA procedure enabled by this approximation is computationally-efficient, as we do not need to solve an SQP for each extra state-action sample $(\mathbf{x}_{t,j}^+, \mathbf{u}_{t,j}^+)$ generated for DA, and we only need to compute, once per timestep, the sensitivity matrix $\mathbf{K}_{\tilde{\boldsymbol{\chi}}_t}$. We note that the feedback-response introduced by the so-generated extra state-action samples can be interpreted as a type of linearized neighboring feedback control [46, §1.3.1], where the linear feedback law is computed based on the trajectory $\boldsymbol{\xi}$ executed during demonstration collection in the source environment \mathcal{S} , rather than a reference trajectory $\mathbf{Z}_{t_0}^*, \mathbf{V}_{t_0}^*$. We remark, additionally, that the actions computed when collecting demonstrations are obtained by solving the entire SQP, and the sensitivity-base approximation is used only for DA.

Sensitivity Matrix Computation. As described in [2, §8.6], an expression to compute the sensitivity matrix in Eq. (18) (also called *tangential predictor*) can be obtained by re-writing the NLP in Eq. (16) in a parametric form $p([\mathbf{x}_t]_i)$, highlighting the dependency on scalar parameter representing the i -th component of the initial state \mathbf{x}_t (part of $\boldsymbol{\chi}_t$). The parametric NLP $p([\mathbf{x}_t]_i)$ is:

$$\begin{aligned} & \min_{\mathbf{y}} F_{\boldsymbol{\chi}_t}(\mathbf{y}) \\ & \text{subject to } G_{\boldsymbol{\chi}_t}([\mathbf{x}_t]_i, \mathbf{y}) = \mathbf{0} \\ & H(\mathbf{y}) \leq \mathbf{0}, \end{aligned} \quad (20)$$

where $\mathbf{y} \in \mathbb{R}^{n_y}$ corresponds to the optimization variables in Eq. (16), and $F_{\boldsymbol{\chi}_t}(\cdot), G_{\boldsymbol{\chi}_t}(\cdot), H(\cdot)$ are, respectively, the objective function, equality, and inequality constraints in Eq. (16), given the current state and reference trajectory in $\boldsymbol{\chi}_t$. Additionally, we denote the solution of Eq. (20) at $\tilde{\boldsymbol{\chi}}_t$ (computed during the collected demonstration) as $(\tilde{\mathbf{y}}^*, \tilde{\boldsymbol{\lambda}}^*, \tilde{\boldsymbol{\mu}}^*)$, where $\tilde{\boldsymbol{\lambda}}^*, \tilde{\boldsymbol{\mu}}^*$ are, respectively, the Lagrange multipliers for the equality and inequality constraints at the solution found. Then, each i -th column of the sensitivity matrix (Eq. (18)) can be computed by solving the following QP ([2, Th. 8.16], and [46, Th. 3.4 and Remark 4]):

$$\begin{aligned} & \min_{\mathbf{y}} F_{\boldsymbol{\chi}_t, L}(\mathbf{y}; \tilde{\mathbf{y}}^*) + \frac{1}{2}(\mathbf{y} - \tilde{\mathbf{y}}^*)^\top \nabla_{\mathbf{y}}^2 \mathcal{L}(\tilde{\mathbf{y}}^*, \tilde{\boldsymbol{\lambda}}^*, \tilde{\boldsymbol{\mu}}^*)(\mathbf{y} - \tilde{\mathbf{y}}^*) \\ & \text{s.t. } G_{\boldsymbol{\chi}_t, L}([\mathbf{x}_t]_i, \mathbf{y}; \tilde{\mathbf{y}}^*) = \mathbf{0} \\ & H_L(\mathbf{y}; \tilde{\mathbf{y}}^*) \leq \mathbf{0} \end{aligned} \quad (21)$$

where $F_{\boldsymbol{\chi}_t, L}(\cdot; \tilde{\mathbf{y}}^*), G_{\boldsymbol{\chi}_t, L}(\cdot; \tilde{\mathbf{y}}^*), H_L(\cdot; \tilde{\mathbf{y}}^*)$ denote the respective functions in Eq. (20) linearized at the solution found. $\nabla_{\mathbf{y}}^2 \mathcal{L}$ denotes the Hessian of the Lagrangian associated with Eq. (20), while the parameter is set to zero ($[\mathbf{x}_t]_i = 0$). The i -th column of the sensitivity matrix can be extracted from the entries of \mathbf{y}^* , solution of Eq. (21), at the position corresponding to $\bar{\mathbf{u}}_{0|t}$. We highlight that Eq. (21) can be computed efficiently, as it leverages the latest internal linearization of the Karush–Kuhn–Tucker (KKT) conditions performed in the SQP employed to solve Eq. (16), and therefore it does not require to re-execute the computationally expensive system linearization routines that are carried out at each SQP iteration. We note that this local approximation exists when the assumptions in [2, Th. 8.15] (equivalent to [46, Th. 3.3]) and [46, Th. 3.3, Remark 2, 4] are satisfied, i.e., that the solution $(\tilde{\mathbf{y}}^*, \tilde{\boldsymbol{\lambda}}^*, \tilde{\boldsymbol{\mu}}^*)$ found during

demonstration collection is a strongly regular KKT point, and the assumptions, i.e., that the solution found satisfies strict complementary conditions. Last, extra samples are generated using Eq. (19) under the assumption that the set of active inequality constraints (i.e., the index set $p \in \{1, \dots, n_H\}$ such that $[H(\tilde{\mathbf{y}}^*)]_p = 0$) does not change.

Generalized Tangential Predictor A strategy that applies to the cases where strict complementary conditions do not hold, or where the extra state samples cause a change in the active set of constraints, is based on the *generalized tangential predictor* [2, §8.9.1]. This predictor can be obtained by solving the QP in Eq. (21) with the set of equality constraints modified to be $G_{\mathbf{x}_t, L}(\mathbf{x}_{t,j}^+, \mathbf{y}; \tilde{\mathbf{y}}) = \mathbf{0}$ [2, Eq. 8.60]. Although this approach requires solving a QP to compute the action $\mathbf{u}_{t,j}^+$ corresponding to each state $\mathbf{x}_{t,j}^+$ sampled from the tube, it does not require re-generating the computationally expensive linearization performed at each SQP iteration (and other performance optimization routines, such as condensing [2]) nor solving the entire SQP for multiple iterations – resulting in a much more computationally-efficient procedure than solving the entire SQP *ex-novo* for every extra state-action sample. We remark that the linearization point in Eq. (21) is updated at every timestep when a full SQP is solved as part of demonstration-collection.

D. Robustness and Performance Under Approximate Samples

While the proposed sensitivity-based DA strategy enables the efficient generation of extra state-action samples, it introduces approximation errors that may affect the performance and robustness of the learned policy. Here, we discuss strategies to account for these errors, reducing the gaps between the nonlinear RTMPC expert and the learned policy in terms of robustness and performance.

Robustness. A key property of RTMPC is the ability to explicitly account for uncertainties, including the ones introduced by the proposed sensitivity-based DA framework, by further tightening state and actuation constraints for the nominal safe plan (Eq. (15)). The general nonlinear formulation of the dynamics in Eq. (1), however, makes it challenging to compute an *exact* additional tightening bound for state and actuation constraints. A possible avenue to establish a tightening procedure for the actuation constraints is to observe that the linear approximation of Eq. (17) introduces an error upper bounded by ([2, Th. 8.16]):

$$\|\kappa(\boldsymbol{\chi}_t) - \hat{\kappa}(\mathbf{x}_{t,j}^+, \boldsymbol{\chi}_t)\| \leq D \|\mathbf{x}_{t,j}^+ - \mathbf{x}_t\|^2 \quad (22)$$

where D may be obtained by considering the Lipschitz constant of the controller (e.g. [39]). However, estimating this constant may be difficult, or computationally expensive, for large-dimensional systems, as is the case herein. An alternative is to update the tubes as was done in Section V-A, e.g., by employing Monte-Carlo simulations of the closed-loop system, starting from an initial (possibly conservative) tightening guess and by iteratively adjusting the cross-section (size) of the tube, or by directly learning the tubes from simulations or previous (conservative) real-world deployments [44]. These procedures, when performed using the learned policy, are

particularly appealing in our context, as our efficient policy learning methodologies enable rapid training/updates of the learned policy, and the computational efficiency of the policy enables rapid simulations.

Performance Improvements via Fine-Tuning In the context of learning policies from nonlinear RTMPC, we include in SA an (optional) fine tuning-step. This fine-tuning step consists in training the policy with additional demonstrations, without DA, therefore avoiding introducing further approximate samples, and having discarded the extra data used to train the policy after an initial demonstration. More specifically, the overall SA procedure for nonlinear RTMPC with the optional fine-tuning step consists of the following:

- 1) Collect a single task demonstration ξ (e.g., reach goal) from the nonlinear RTMPC expert;
- 2) Perform DA using the parametric sensitivity (Section V-C) and train the policy, obtaining the policy parameters $\hat{\theta}_0$;
- 3) Optional *fine-tuning* step:
 - i) Discard the collected data so far, including the data generated by the DA;
 - ii) Collect new demonstrations (e.g., using DAgger [16] and the pre-trained policy, or BC), without DA, and re-train the pre-trained policy (with parameters $\hat{\theta}_0$) after every newly collected demonstration.

In this procedure, our proposed tube-guided DA is treated as a methodology to efficiently generate an initial guess $\hat{\theta}_0$ of the policy parameters; the policy can then be further fine-tuned, for performance improvements, using newly collected demonstrations via on-policy (e.g. DAgger) or off-policy methods (e.g., BC).

VI. APPLICATION TO AGILE FLIGHT

In this Section, we tailor the proposed efficient policy learning strategies to agile flight tasks, as this will be the focus of our numerical and experimental evaluation. First, in Section VI-A, we present the nonlinear model of the multirotor used to collect demonstrations in simulation in all our approaches, and used for control design. Then, in Section VI-B, we present a RTMPC expert for *trajectory tracking* based on a *linear* multirotor model and that will be used with the IL procedure described in Section IV. Because the considered trajectories require the robot to operate around a fixed, pre-defined condition (near hover), a hover-linearized model is suitable for the design of this controller. Last, in Section VI-C, we design a nonlinear RTMPC expert capable of performing a 360° flip in *near-minimum time* - a maneuver that demands exploitation of the full *nonlinear* dynamics of the multirotor, and that requires large and careful actuation usage. This controller will be used with the IL procedure described in Section V.

A. Nonlinear Multirotor Model

We consider an inertial reference frame \mathbf{W} attached to the ground, and a non-inertial frame \mathbf{B} attached to the center of

mass (CoM) of the robot. The translational and rotational dynamics of the multirotor are:

$${}_{\mathbb{W}}\dot{\mathbf{p}} = {}_{\mathbb{W}}\mathbf{v} \quad (23a)$$

$${}_{\mathbb{W}}\dot{\mathbf{v}} = m^{-1}(\mathbf{R}_{\mathbb{W}\mathbb{B}} \mathbf{t}_{\text{cmd}} + {}_{\mathbb{W}}\mathbf{f}_{\text{drag}} + {}_{\mathbb{W}}\mathbf{f}_{\text{ext}}) - {}_{\mathbb{W}}\mathbf{g} \quad (23b)$$

$$\dot{\mathbf{q}}_{\mathbb{W}\mathbb{B}} = \frac{1}{2} \boldsymbol{\Omega}({}_{\mathbb{B}}\boldsymbol{\omega}) \mathbf{q}_{\mathbb{W}\mathbb{B}} \quad (23c)$$

$${}_{\mathbb{B}}\dot{\boldsymbol{\omega}} = \mathbf{I}_{\text{mav}}^{-1}(-{}_{\mathbb{B}}\boldsymbol{\omega} \times \mathbf{I}_{\text{mav}} {}_{\mathbb{B}}\boldsymbol{\omega} + {}_{\mathbb{B}}\boldsymbol{\tau}_{\text{cmd}} + {}_{\mathbb{B}}\boldsymbol{\tau}_{\text{drag}}) \quad (23d)$$

where \mathbf{p} , \mathbf{v} , \mathbf{q} , $\boldsymbol{\omega}$ are, respectively, position, velocity, attitude quaternion and angular velocity of the robot, with the prescript denoting the corresponding reference frame. The attitude quaternion $\mathbf{q} = [q_w, \mathbf{q}_v^\top]^\top$ consists of a scalar part q_w and a vector part $\mathbf{q}_v = [q_x, q_y, q_z]^\top$ and it is unit-normalized; the associated 3×3 rotation matrix is $\mathbf{R} = \mathbf{R}(\mathbf{q})$, while

$$\boldsymbol{\Omega}(\boldsymbol{\omega}) = \begin{bmatrix} 0 & -\boldsymbol{\omega}^\top \\ \boldsymbol{\omega} & [\boldsymbol{\omega}]_\times \end{bmatrix}, \quad (24)$$

with $[\boldsymbol{\omega}]_\times$ denoting the 3×3 skew symmetric matrix of $\boldsymbol{\omega}$. m denotes the mass, \mathbf{I}_{mav} the 3×3 diagonal inertial matrix, and $\mathbf{g} = [0, 0, g]^\top$ the gravity vector. Aerodynamic effects are taken into account via $\mathbf{f}_{\text{drag}} = -c_{D,1}\mathbf{v} - c_{D,2}\|\mathbf{v}\|\mathbf{v}$ and isotropic drag torque $\boldsymbol{\tau} = -c_{D,3}\boldsymbol{\omega}$, capturing the parasitic drag produced by the motion of the robot. The robot is additionally subject to external force disturbances \mathbf{f}_{ext} , such as the one caused by wind or by an unknown payload. Last, $\mathbf{t}_{\text{cmd}} = [0, 0, t_{\text{cmd}}]^\top$ is the commanded thrust force, and $\boldsymbol{\tau}_{\text{cmd}}$ the commanded torque. These commands can be mapped to the desired thrust $f_{\text{prop},i}$ for the i -th propeller ($i = 1, \dots, n_p$) via a linear mapping (allocation matrix) \mathcal{A} :

$$\begin{bmatrix} t_{\text{cmd}} \\ \boldsymbol{\tau}_{\text{cmd}} \end{bmatrix} = \mathcal{A} \begin{bmatrix} f_{\text{prop},1} \\ \vdots \\ f_{\text{prop},n_p} \end{bmatrix} = \mathcal{A} \mathbf{f}_{\text{prop}}. \quad (25)$$

The attitude of the quadrotor is controlled via the geometric attitude controller in [47] that generates desired torque commands ${}_{\mathbb{B}}\boldsymbol{\tau}_{\text{cmd}}$ given a desired attitude $\mathbf{R}_{\mathbb{W}\mathbb{B}}^{\text{des}}$, angular velocity ${}_{\mathbb{B}}\boldsymbol{\omega}^{\text{des}}$ and acceleration ${}_{\mathbb{B}}\dot{\boldsymbol{\omega}}^{\text{des}}$. The controllers designed in the next sections output setpoints for the attitude controller, and desired thrust t_{cmd} .

B. Linear RTMPC for Trajectory Tracking

The model employed by the linear RTMPC for trajectory tracking (Eq. (10)) is based on a simplified, hover-linearized model derived from Eq. (27), using the approach in [6], but modified to account for uncertainties. First, similar to [6], we express the model in a yaw-fixed, gravity-aligned frame I via the rotation matrix \mathbf{R}_{BI}

$$\begin{bmatrix} \phi \\ \theta \end{bmatrix} = \mathbf{R}_{\text{BI}} \begin{bmatrix} I\phi \\ I\theta \end{bmatrix}, \quad \mathbf{R}_{\text{BI}} = \begin{bmatrix} \cos(\psi) & \sin(\psi) \\ -\sin(\psi) & \cos(\psi) \end{bmatrix}, \quad (26)$$

where the attitude has been represented, for interpretability, via the Euler angles yaw ψ , pitch θ , roll ϕ (*intrinsic* rotations around the z - y - x such that $\mathbf{R} = \mathbf{R}_z(\psi) \mathbf{R}_y(\theta) \mathbf{R}_x(\phi)$, with $\mathbf{R}_l(\alpha)$ being a rotation of α around the l -th axis). Second, as in [6], we assume that the closed-loop attitude dynamics can be described by a first-order dynamical system that can

be identified from experiments, replacing Eq. (23c), Eq. (23d). Last, different from [6], we assume ${}_{\mathbb{W}}\mathbf{f}_{\text{ext}}$ in Eq. (23b) to be an unknown disturbance/model errors that capture the uncertain parts of the model, such that ${}_{\mathbb{W}}\mathbf{f}_{\text{ext}} \in \mathbb{W}$.

The controller generates tilt (roll, pitch) and thrust commands ($n_u = 3$) given the state of the robot ($n_x = 8$) consisting of position, velocity, and tilt, and given the reference trajectory. The desired yaw is fixed (and it is tracked by the cascaded attitude controller); similarly, ${}_{\mathbb{B}}\boldsymbol{\omega}^{\text{des}}$ and ${}_{\mathbb{B}}\dot{\boldsymbol{\omega}}^{\text{des}}$ are set to zero. We employ the nonlinear attitude compensation scheme in [6].

The controller takes into account position constraints (e.g., available 3D flight space), actuation limits, and velocity/tilt limits via \mathbb{X} and \mathbb{U} . The cross-section of the tube \mathbb{Z} is a constant outer approximation based on an axis-aligned bounding box. It is estimated via Monte-Carlo sampling, by measuring the state deviations of the closed loop linear system \mathbf{A}_K under the disturbances in \mathbb{W} .

C. Nonlinear RTMPC for Acrobatic Maneuvers

Ancillary NMPC. We start by designing the ancillary NMPC (Eq. (16)). The selected nominal model is the same used in the high-performance trajectory tracking NMPC for multirotors [18], [48]:

$$\begin{aligned} {}_{\mathbb{W}}\dot{\mathbf{v}} &= m^{-1}(\mathbf{R}_{\mathbb{W}\mathbb{B}} \mathbf{t}_{\text{cmd}} + {}_{\mathbb{W}}\mathbf{f}_{\text{drag}}) - {}_{\mathbb{W}}\mathbf{g} \\ {}_{\mathbb{W}}\dot{\mathbf{p}} &= {}_{\mathbb{W}}\mathbf{v} \\ \dot{\mathbf{q}}_{\mathbb{W}\mathbb{B}} &= \frac{1}{2} \boldsymbol{\Omega}({}_{\mathbb{B}}\boldsymbol{\omega}_{\text{cmd}}) \mathbf{q}_{\mathbb{W}\mathbb{B}}, \end{aligned} \quad (27)$$

where the rotational dynamics (Eq. (23d)) have been neglected, assuming that the cascaded attitude controller enables fast tracking of the desired angular velocity setpoint ${}_{\mathbb{B}}\boldsymbol{\omega}_{\text{cmd}}$. The controller uses the state and control input:

$$\bar{\mathbf{x}} = [{}_{\mathbb{W}}\mathbf{p}^\top, {}_{\mathbb{W}}\mathbf{v}^\top, \mathbf{q}_{\mathbb{W}\mathbb{B}}^\top]^\top, \quad \bar{\mathbf{u}} = [t_{\text{cmd}}, {}_{\mathbb{B}}\boldsymbol{\omega}_{\text{cmd}}^\top]^\top. \quad (28)$$

The angular acceleration setpoint for the attitude controller ${}_{\mathbb{B}}\dot{\boldsymbol{\omega}}_{\text{cmd}}$ is obtained via numerical differentiation, while we do not explicitly generate an attitude setpoint (e.g., we set $\mathbf{R}_{\mathbb{W}\mathbb{B}}^{\text{des}} = \mathbf{R}_{\mathbb{W}\mathbb{B}}$) obtaining an attitude controller that only tracks desired angular velocities/accelerations.

Near-Minimum Time Safe Plan Generation. To compute safe nominal plans for acrobatic maneuvers (by solving the OCP in Eq. (15)), we employ an extended version of the full nonlinear dynamic model in Section VI-A. More specifically, we solve the OCP in Eq. (15) by using the following state $\tilde{\mathbf{z}} \in \tilde{\mathbb{Z}}$ and control inputs $\tilde{\mathbf{v}} \in \tilde{\mathbb{V}}$:

$$\tilde{\mathbf{z}} = [{}_{\mathbb{W}}\mathbf{p}^\top, {}_{\mathbb{W}}\mathbf{v}^\top, \mathbf{q}_{\mathbb{W}\mathbb{B}}^\top, {}_{\mathbb{B}}\boldsymbol{\omega}^\top, \mathbf{f}_{\text{prop}}^\top]^\top, \quad \tilde{\mathbf{v}} = {}_{\mathbb{B}}\dot{\mathbf{f}}_{\text{prop}}, \quad (29)$$

where the state has been extended to include the thrust produced by each propeller \mathbf{f}^{prop} to ensure continuity in the reference thrust, accounting for the unmodeled actuators' dynamics. As for the linear case, uncertainties are modeled by ${}_{\mathbb{W}}\mathbf{f}_{\text{ext}} \in \mathbb{W}$. The cost function captures the near-minimum time objective:

$$\tilde{J}_{\text{RTNMPC}} = T_f + \alpha_1 \mathbf{v}^\top \mathbf{v} + \alpha_2 \mathbf{f}_{\text{prop}}^\top \mathbf{f}_{\text{prop}} + \alpha_3 \tilde{\mathbf{v}}^\top \tilde{\mathbf{v}} \quad (30)$$

where T_f is the total time of the maneuver, while the remaining terms act as a regularizer for the optimizer, with $\alpha_i \ll T_f$ (i.e., $\alpha_i \approx 10^{-2}$, $\forall i$).

We note that $\tilde{J}_{\text{RTNMPC}}$ contains a non-quadratic term, therefore differing from the quadratic cost employed in the safe nominal planner in [36] (our Eq. (15)); such cost function was chosen to automate the selection of the prediction horizon N for the safe nominal plan. Our evaluation will demonstrate that the ancillary NMPC maintains the system within a tube from the generated reference, further highlighting the flexibility of the framework.

Additionally, we note that state and control input (Eq. (29)) have been extended compared to the ones (Eq. (28)) selected for the ancillary NMPC, as emphasized by our notation $\tilde{\cdot}$. For this reason, the optimal safe nominal plan $\tilde{\mathbf{Z}}_t^*$, $\tilde{\mathbf{V}}_t^*$ found using the extended state needs to be mapped to the reference trajectory for the ancillary NMPC, \mathbf{Z}_t^* , \mathbf{V}_t^* . This is done by simply selecting position, velocity and attitude from $\tilde{\mathbf{Z}}_t^*$ to obtain \mathbf{Z}_t^* . The thrust setpoint t_{cmd} in \mathbf{V}_t^* is computed via \mathcal{A} in Eq. (25) from \mathbf{f}_{prop} in $\tilde{\mathbf{Z}}_t^*$, while the angular velocity setpoint $\boldsymbol{\omega}_{\text{cmd}}$ is obtained by assuming it equal to the angular velocity $\boldsymbol{\omega}$ in $\tilde{\mathbf{Z}}_t^*$.

Constraints. The state constraint $\bar{\mathbf{x}}_t \in \mathbb{X}$ encodes the maximum safe linear velocity \mathbf{v} and position boundaries \mathbf{p} of the environment, while actuation constraints $\bar{\mathbf{u}}_t \in \mathbb{U}$ account for physical limits of the robot, restricting the nominal angular velocities $\boldsymbol{\omega}_{\text{cmd}}$ (to prevent saturation of the onboard gyroscope), and the maximum/minimum thrust force t_{cmd} produced by the propellers. We impose tightened constraints on the thrust force by constraining \mathbf{f}_{prop} in $\tilde{\mathbf{z}} \in \tilde{\mathbb{Z}}$. These constraints are obtained via a conservative approach, i.e. we require a minimal thrust to generate a trajectory feasible within our position and velocity constraints. This was done to ensure that sufficient control authority is left to the ancillary NMPC to account for the presence of large unknown aerodynamic effects and mismatches in the mapping from commanded thrust/actual thrust. This cautious approach enabled successful real-world execution of the maneuver without further real-world tuning. We additionally leverage the further degrees of freedom introduced by the extended state $\tilde{\mathbf{z}}$ by shaping the safe plan through upper-bounding the thrust rates $\dot{\mathbf{f}}_{\text{prop}}$ via $\tilde{\mathbf{V}}$, although this constraint will not be enforced by the ancillary NMPC. Last, using Monte-Carlo closed-loop simulations with disturbances sampled from \mathbb{W} , we verify that \mathbb{X} and \mathbb{U} are satisfied, and we generate a constant estimate (outer approximation, axis-aligned bounding box) of the cross-section of the tubes $\mathbb{T}^{\text{state}}$ and $\mathbb{T}^{\text{action}}$.

Tube and Data Augmentation with Attitude Quaternions. The normalized attitude quaternion, part of the states $\bar{\mathbf{x}}$, $\tilde{\mathbf{z}}$ of nonlinear RTMPC, and part of the reference \mathbf{Z}_t^* for the ancillary NMPC, does not belong to a vector space, and therefore it is not trivial to describe its tube nor to generate extra samples for DA. In this work, we employ an attitude error representation $\boldsymbol{\epsilon} \in \mathbb{R}^3$ based on the Modified Rodriguez Parameters (MRP) [49] to generate a representation that can be treated as an element of a vector space. Specifically, we use

$$\boldsymbol{\epsilon}_t = \text{MRP}(\mathbf{q}_t \odot \mathbf{q}_t^{*-1}), \quad (31)$$

where \mathbf{q}_t is the current attitude, \mathbf{q}_t^* is the desired attitude (from the safe plan \mathbf{z}_t^*), $\text{MRP}(\cdot)$ maps a quaternion to the corresponding three-dimensional attitude representation, while \odot denotes the quaternion product.

VII. EVALUATION - LEARNING FROM LINEAR RTMPC

We start by evaluating our policy learning approach for the task of trajectory tracking using the linear RTMPC expert.

A. Evaluation Approach and Details

Simulation Environment. Demonstration collection and policy evaluations are performed in a simulation environment implementing the nonlinear multirotor dynamics in Section VI-A, discretized at 200Hz, while the attitude controller runs at 100Hz. The robot follows desired trajectories, starting from randomly generated initial states centered around the origin. Given the specified external disturbance magnitude bound $\mathbb{W}_{\mathcal{D}} = \{f_{\text{ext}} \in \mathbb{R} \mid \underline{f}_{\text{ext}} \leq f_{\text{ext}} \leq \bar{f}_{\text{ext}}\}$, disturbances are applied in the domain \mathcal{D} by sampling ${}_w\mathbf{f}_{\text{ext}}$ via the spherical coordinates:

$${}_w\mathbf{f}_{\text{ext}} = f_{\text{ext}} \begin{bmatrix} \cos(\phi) \sin(\theta) \\ \sin(\phi) \sin(\theta) \\ \cos(\theta) \end{bmatrix}, \quad \begin{aligned} f_{\text{ext}} &\sim \mathcal{U}(\underline{f}_{\text{ext}}, \bar{f}_{\text{ext}}), \\ \theta &\sim \mathcal{U}(0, \pi), \\ \phi &\sim \mathcal{U}(0, 2\pi). \end{aligned} \quad (32)$$

Linear RTMPC. The linear RTMPC demonstrator runs at 10Hz. The reference fed to the expert is a sequence of desired positions and velocities for the next 3s, discretized with a sampling time of 0.1s; the expert uses a corresponding planning horizon of $N = 30$, (resulting in a reference being a 180-dim. vector). The controller is designed under the assumption that $\mathbb{W} = \{f_{\text{ext}} \in \mathbb{R} \mid 0 \leq f_{\text{ext}} \leq 0.3mg\}$, corresponding to the safe physical limit of the actuators of the robot.

Policy Architecture. The student policy is a 2-hidden layer, fully connected DNN, with 32 neurons per layer, and ReLU activation function. The total input dimension of the DNN is 188 (matching the input of the expert, consisting of state and reference trajectory). The output dimension is 3 (desired thrust and tilt expressed in an inertial frame). We rotate the tilt output of the DNN in the body frame to avoid taking into account yaw, which is not part of the optimization problem [6], not causing any relevant computational cost. We additionally apply the nonlinear attitude compensation scheme as in [6].

Baselines and Training Details. We apply the proposed SA strategies to every demonstration collected via DAGger or BC, and compare their performance against the two without SA and the two combined with DR. During demonstration-collection in the source environment \mathcal{S} , we do not apply disturbances, setting $\mathbb{W}_{\mathcal{S}} = \{\emptyset\}$, with the exception for DR, where we sample disturbances from $\mathbb{W}_{\text{DR}} = \mathbb{W}_{\mathcal{T}}$. In all the methods that use DAGger we set the probability of using actions of the expert β (a hyperparameter of DAGger [16]) to be 1 at the first demonstration and 0 otherwise (as this was found to be the best-performing setup). Demonstrations are collected with a sampling time of 0.1s. After every collected demonstration, the policy is trained for 50 epochs² using all the data available so far with the ADAM [50] optimizer and a learning rate of 0.001. The policy is then evaluated on the task for 20 times (episodes), starting from slightly different initial states centered around the origin, in both \mathcal{S} and \mathcal{T} .

Evaluation Metrics: We monitor:

²One epoch is one pass through the entire dataset

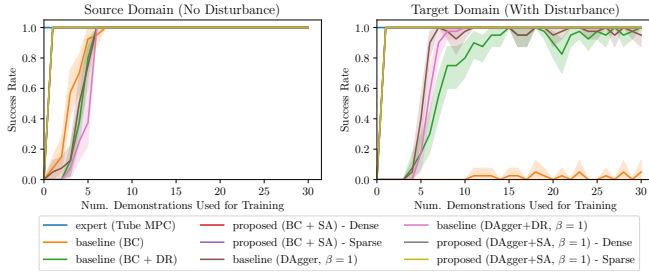


Fig. 5: Robustness (*Success Rate*) in the task of flying along an eight-shaped, 7s long-trajectory, subject to wind-like disturbances (right, target domain \mathcal{T}_1) and without (left, source domain \mathcal{S}), starting from different initial states. Evaluation is repeated across 8 random seeds, 20 times per demonstration per seed. We additionally show the 95% confidence interval. The lines for the SA-based methods overlap.

TABLE I: Comparison of the IL methods considered to learn a policy from RTMPC. We consider the task of tracking a trajectory in a deployment domain with wind-like disturbances (\mathcal{T}_1), and one under model errors (\mathcal{T}_2 , under drag coefficient mismatch). At convergence (iteration 20-30) we evaluate robustness (success rate) and performance (relative percent error between tracking error of expert and policy). Demonstration-Efficiency represents the number of demonstrations required to achieve, for the first time, full success rate. An approach is considered easy if it does not require to apply disturbances/perturbations during training (e.g., in *lab2real* transfer); an approach is considered safe if does not execute actions that may cause state constraints violations (crashes) during training. *Safe in our numerical evaluation, but not guaranteed as it requires executing actions of a policy that may be partially trained.

Method	Training		Robustness succ. rate (%)		Performance expert gap (%)		Demonstration Efficiency		
	Robustif.	Imitation	Easy	Safe	\mathcal{T}_1	\mathcal{T}_2	\mathcal{T}_1	\mathcal{T}_2	
-	BC	Yes	Yes	< 1	100	24.15	29.47	-	6
	Dagger	Yes	No	98	100	15.79	1.34	7	6
DR	BC	No	Yes	95	100	10.04	1.27	14	9
	Dagger	No	No	100	100	4.09	1.45	10	6
SA-Dense	BC	Yes	Yes	100	100	25.64	1.34	1	1
	Dagger	Yes	Yes*	100	100	10.21	1.66	1	1
SA-Sparse	BC	Yes	Yes	100	100	4.23	1.13	1	1
	Dagger	Yes	Yes*	100	100	3.75	1.07	1	1

- i) *Robustness (Success Rate)*, as the percentage of episodes where the robot never violates any state constraint;
- ii) *Performance*, via either
 - a) $C_{\xi}(\pi_{\theta}) := \sum_{t=0}^T \|\mathbf{x}_t - \mathbf{x}_t^{\text{des}}\|_{\mathbf{Q}_x}^2 + \|\mathbf{u}_t\|_{\mathbf{R}_u}^2$ tracking error along the trajectory (*MPC Stage Cost*); or
 - b) $\|C_{\xi}(\pi_{\theta^*}) - C_{\xi}(\pi_{\hat{\theta}^*})\| / \|C_{\xi}(\pi_{\theta^*})\|$ relative error between expert and policy tracking errors (*Expert Gap*);
- iii) *Efficiency*
 - a) number of expert demonstrations (*Num. Demonstrations Used for Training*), and
 - b) wall-clock time to generate the policy (*Training Time*³).

B. Numerical Evaluation of Demonstration-Efficiency, Robustness, and Performance when Learning to Track a Single Trajectory

Tasks Description. Our objective is to generate a policy from linear RTMPC capable of tracking a 7s long (70 steps), figure eight-shaped trajectory. We evaluate the considered IL approaches in two different target domains, with wind-like disturbances (\mathcal{T}_1) or with model errors (\mathcal{T}_2). Disturbances in \mathcal{T}_1 are external force perturbations \mathbf{f}_{ext} sampled from $\mathbb{W}_{\mathcal{T}_1} \approx \{\mathbf{f}_{\text{ext}} | 0.25mg \leq \mathbf{f}_{\text{ext}} \leq 0.3mg\}$. Model errors in \mathcal{T}_2 are applied via mismatches in the drag coefficients used between

³Training time is the time to collect demonstrations and the time to train the policy, as measured by a wall-clock. In our evaluations, the simulated environment steps at its highest possible rate (in contrary to running at the same rate of the simulated physical system), providing an advantage to those methods that require a large number of environment interactions, such as the considered baselines.

TABLE II: Computation time required to generated a new action for the linear RTMPC (Expert) and the DNN policy (Policy). The DNN policy is 25.2 times faster than the optimization-based expert. Evaluation performed on an Intel i9-10920.

Method	Setup	Time (ms)			
		Mean	St. Dev.	Min	Max
Expert (Linear)	CVXPY [51]	4.28	0.39	4.21	16.66
Policy	PyTorch	0.17	0.00	0.17	0.22

training and testing, representing uncertainties not explicitly considered during the design of the linear RTMPC.

Results. We start by evaluating the robustness in \mathcal{T}_1 as a function of the number of demonstrations collected in the source domain. The results are shown in Fig. 5, highlighting that: i) while all the approaches achieve robustness (full success rate) in the source domain, SA achieves full success rate after only a single demonstration, being 5-6 times more sample efficient than the baseline methods; ii) SA is able to achieve full robustness in the target domain, while baseline methods do not fully succeed, and converge at a much lower rate. These results emphasize the presence of a distribution shift between the source and target, which is not fully compensated for by baseline methods such as BC due to a lack of exploration and robustness.

The performance evaluation and additional results are summarized in Table I. We highlight that in the target domain \mathcal{T}_1 , SA-sparse combined with DAgger achieves the performance that is closest to the expert. SA-dense suffers from performance drops, potentially due to the limited capacity of the considered DNN or challenges in training introduced by this DA. Table I additionally presents the results for the target domain \mathcal{T}_2 . Although this task is less challenging (i.e., all the approaches achieve full robustness), the proposed method (SA-sparse) achieves the highest demonstration-efficiency and lowest expert gap, with similar trends as in \mathcal{T}_1 .

Training Time. Fig. 5 highlights that the best-performing baseline, DAgger+DR, requires about 10 demonstrations to learn to robustly track a 7s long trajectory, which corresponds to a total training time of 10.8s. Among the proposed approaches, DAgger+SA-sparse instead only requires 1 demonstration, corresponding to a training time of 3.8s, a 64.8% reduction in wall-clock time required to learn the policy. DAgger+SA-dense, instead, while requiring a single demonstration to achieve full robustness, necessitates 114s of training time due to the large number of samples generated. Because of its effectiveness and greater computational efficiency, we use SA-sparse, rather than SA-dense, for the rest of the work.

Computation. Table II shows that the DNN policy is about 25 times faster than the expert. We additionally report that the average latency for the policy on an Nvidia Jetson TX2 (CPU, PyTorch) is 1.66ms.

C. Hardware Evaluation for Tracking a Single Trajectory from a Single Demonstration

Sim2Real Transfers. We validate the demonstration-efficiency, robustness, and performance of the proposed approach by experimentally testing policies trained after a *single* demonstration collected in simulation using DAgger/BC (which operate identically since we use DAgger with $\beta = 1$ for

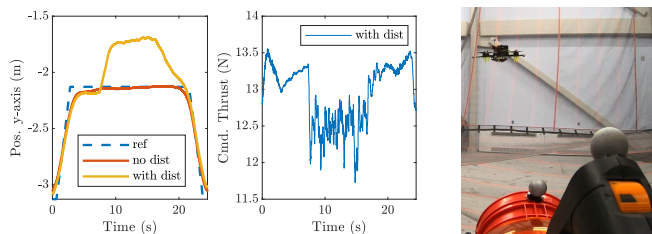


Fig. 6: Experimental evaluation performed by hovering with and without wind disturbances produced by a leaf blower. The employed policy is trained in simulation from a *single* demonstration of the desired trajectory. The wind-like disturbances produce a large position error but do not destabilize the system. The thrust decreases due to the robot being pushed up by the disturbances. The state estimate (shown in the plot) is provided by onboard VIO. The wind points approximately in the same direction as the y -axis.

the first demonstration), combined with SA-sparse. We use the MIT/ACL open-source snap-stack [52] for controlling the attitude of the MAV. The learned policy runs at 100Hz on the onboard Nvidia Jetson TX2 (CPU), with the reference trajectory provided at 100Hz. State estimation is obtained via a motion capture system or onboard Visual-Inertial Odometry (VIO).

The first task considered is to hover under wind disturbances produced by a leaf blower. The results (Fig. 6) highlight the ability of the system to remain stable despite the large position error caused by the wind.

The second task is to track a figure eight-shaped trajectory, with velocities up to 3.4m/s. We evaluate the robustness of the learned policy by applying a wind-like disturbance produced by an array of 3 leaf blowers (Fig. 7). The given position reference and the corresponding trajectory are shown in Fig. 7a. The effects of the wind disturbances are clearly visible in the altitude errors and changes in commanded thrust in Fig. 7a (at $t = 11$ s and $t = 23$ s). These experiments show that the learned policy can robustly track the desired reference, withstanding challenging perturbations unseen during the training phase.

Lab2Real Transfer. We evaluate the ability of the proposed method to learn from a single demonstration collected on a real robot in a controlled environment (lab) and generalize to previously unseen disturbances (real). We do so by collecting a RTMPC demonstration of a 1m position-step on x - y - z axes of \mathbb{W} with the multirotor, augmenting the collected demonstration with SA-sparse, and deploying the learned policy while we apply previously unseen wind disturbances. As shown in the sequence in Fig. 8 and in our video submission, the policy reproduces the expert demonstration and it is robust to previously unseen wind disturbances.

D. Numerical and Hardware Evaluation for Learning and Generalizing to Multiple Trajectories

We evaluate the ability of the proposed approach to track multiple trajectories while generalizing to unseen ones. To do so, we define a training distribution of reference trajectories (circle, position step, eight-shape) and a distribution for these trajectory parameters (radius, velocity, position). During training, we sample at random a desired, 7s long (70 steps) reference with randomly sampled parameters, collecting a demonstration and updating the proposed policy, while testing on a set of 20, 7s long trajectories randomly sampled from the defined distributions. We monitor the robustness and

TABLE III: Parameters employed for the solution of the ancillary NMPC using the optimization package ACADOS [53].

Parameter	Value
Hessian Approximation	Gauss-Newton
QP solver	Partial Condensing HP-IPM [54]
NLP Tolerance	10^{-8}
QP Tolerance	10^{-8}
Levenberg-Marquardt	10^{-4}
Integrator Type	Implicit Runge-Kutta
Max. # Iterations QP Solver	100
Prediction Horizon (N , steps)	50
Prediction Horizon (time, seconds)	1.0

performance of the different methods, with force disturbances (from $\mathbb{W}_{\mathcal{T}_1}$) applied in the target domain. The results of the numerical evaluation, shown in Fig. 9, confirm that SA-sparse i) achieves robustness and performance comparable to the expert in a sample efficient way, requiring fewer than half the number of demonstrations needed for the baseline approaches; ii) simultaneously learns to generalize to multiple trajectories randomly sampled from the training distribution. The hardware evaluation, performed with DAgger augmented via SA-sparse, is shown in Fig. 10. It confirms that the obtained policy is experimentally capable of tracking multiple trajectories under real-world disturbances/model errors.

VIII. EVALUATION - LEARNING FROM NONLINEAR RTMPC

In this Section, we evaluate the ability of our method to efficiently learn acrobatic flight maneuvers using demonstrations collected from nonlinear RTMPC.

A. Evaluation Approach

Task Description We consider the task of learning a policy capable of performing a flip, i.e., a 360° rotation about the body-frame x -axis, in near-minimum time. This is a challenging maneuver, as it covers a large nonlinear envelope of the dynamics of the Micro Aerial Vehicle (MAV), and the near-minimum time objective function, combined with the need to account for uncertainties, pushes the actuators close to their physical limits.

Simulation Environment. The simulation environment for training/numerical evaluations is the same as in Section VII, i.e., implements the nonlinear multirotor model in Section VI-A. In the training domain (source, \mathcal{S}), $\mathbb{W}_{\mathcal{S}} = \{\emptyset\}$, while in the deployment domain (target, \mathcal{T}) $\mathbb{W}_{\mathcal{T}} = \{f_{\text{ext}} | 0.001mg \leq f_{\text{ext}} \leq 0.3mg\}$, sampled according to Eq. (32).

Nonlinear RTMPC. We generate a safe nominal flip trajectory using MECO-Rocket [55]. Because this nominal trajectory happens in the plane spanned by the orthogonal vectors defining the y and z axis of the inertial reference frame \mathbb{W} , for simplicity, we project the dynamics onto the y and z axes, resulting in a two-dimensional model of the MAV used to generate the nominal plan. The nominal flip trajectory can therefore be obtained by setting the initial rotation around the z to be 0, and the desired final attitude to be 2π , while the remaining initial/terminal states are all set to zero.

The ancillary NMPC is solved using the SQP solver ACADOS [53], and runs in simulation at 50Hz. Sensitivities for DA (Eq.

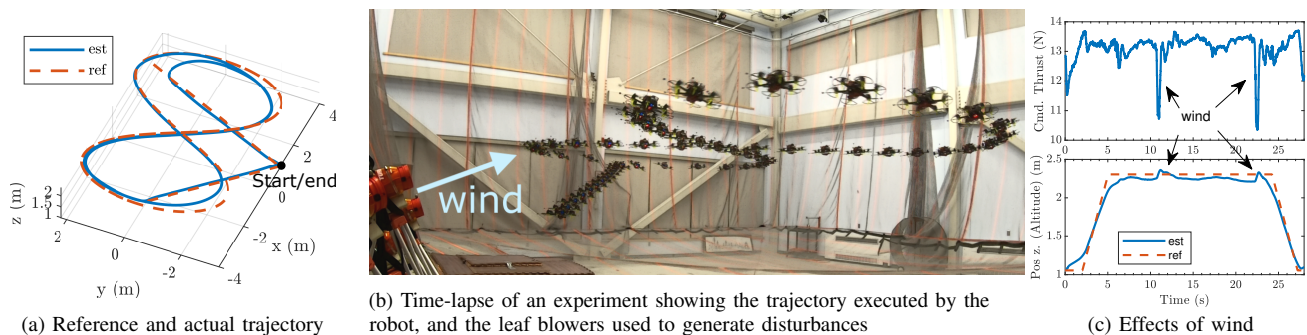


Fig. 7: Experimental evaluation of a trajectory tracking policy learned from a *single* linear RTMPC demonstration collected in simulation, achieving *zero-shot* transfer. The multirotor is able to withstand previously unseen disturbances, such as the wind produced by an array of leaf-blowers, and whose effects are clearly visible in the altitude errors (and change in commanded thrust) in Fig. 7c. This demonstration-efficiency and robustness is enabled by Sampling-Augmentation (SA), our proposed tube-guided data augmentation strategy.



- 1) Demonstration from RTMPC expert, no disturbances
- 2) Student policy reproduces expert demonstration
- 3) Student policy is robust to previously unseen disturbances

Fig. 8: Example of *lab2real* transfer. One expert demonstration (1m step in x - y - z)(1) is sufficient to train a policy that can reproduce the demonstration of the expert (2) and that is robust to previously unseen wind disturbances, accumulating tracking error but not drifting away (3).

(21)) are computed using the built-in sensitivity computation in the chosen solver, HPIPM [54]. We remark that the employed ancillary NMPC uses the full 3D multirotor model in Eq. (27), therefore performing 3D disturbance rejection – a critical requirement for real-world deployments. For a more challenging and interesting comparison to the considered IL baselines, the ancillary NMPC uses the `SQP_RTI` setting of ACADOS. This setting performs only a single SQP iteration per timestep, enabling significant speed-ups in the solver, and it is often employed in real-time, embedded implementations of NMPC. This setting creates an advantage, in terms of training time, to IL methods that require querying the expert multiple times (the baselines of our comparison), as it speeds-up the computation time of the expert. The other ACADOS parameters given in Table III were chosen as they enabled higher overall performance/accuracy in the selected acrobatic maneuver. Last, we introduce a discount factor $\gamma = 0.95$ in the stage cost of Eq. (16) to aid the convergence of the solver.

Student Policy The student policy is a 2-hidden layer, fully connected DNN with $\{64, 32\}$ neurons per layer, and ReLU activation functions. The input vector has dimension 14, as it contains the current state ($n_x = 10$), the current time t , and a desired final position \mathbf{p}^{des} (fixed to the origin). To simplify the learning and DA procedure, we enforce continuity to the quaternion input of the policy using the method in [56, Eq. 3], avoiding the need to increase the training data/demonstrations at every timestep to account for the fact that \mathbf{q} and $-\mathbf{q}$ encode the same orientation.

Baselines and Evaluation Metrics The choice of baselines matches those in Section VII (Dagger, BC and their combination with DR) and so do the monitored metrics (*Robustness*,

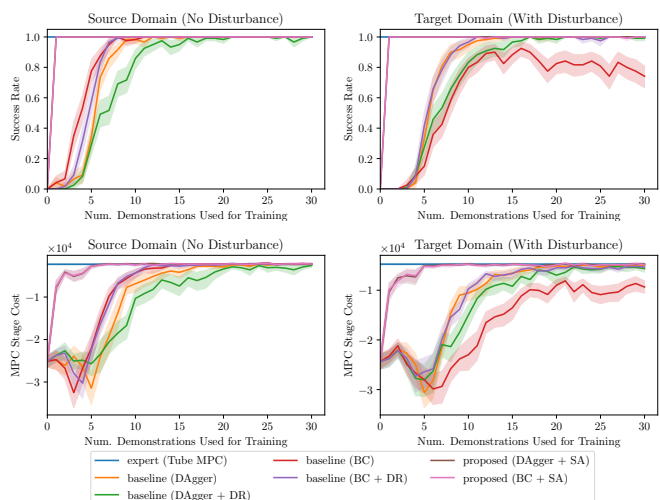


Fig. 9: Robustness (*Success Rate*, top row) and performance (*MPC Stage Cost*, bottom row) of the proposed approach (with 95% confidence interval), as a function of the number of demonstrations used for training, for the task of learning to track previously unseen circular, eight-shaped and constant position reference trajectories, sampled from the same training distribution. The lines for SA-based methods overlap. The left column presents the results in the training domain (no disturbance), while the right column in the target domain, under wind-like perturbations (with disturbance). The proposed RTMPC-driven SA-sparse strategy learns to track multiple trajectories and generalize to unseen ones requiring fewer demonstrations. At convergence (from demonstration 20 to 30), Dagger+SA achieves the closes performance to the expert (2.7% *expert gap*), followed by BC+SA (3.0% *expert gap*). Evaluation performed using 20 randomly sampled trajectories per demonstration, repeated across 6 random seeds, with a prediction horizon of $N = 20$ to speed up demonstration collection, and the DNN input size is adjusted accordingly.

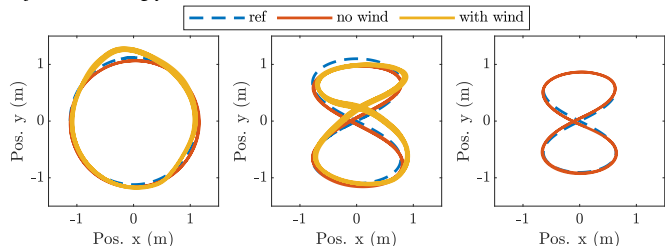


Fig. 10: Examples of different, arbitrary chosen trajectories from the training distribution, tested in hardware experiments with and without strong wind-like disturbances produced by leaf blowers. The employed policy is trained with 10 demonstrations (when other baseline methods have not fully converged yet, see Fig. 9) using Dagger+SA (sparse). This highlights that sparse SA can learn multiple trajectories in a more sample-efficient way than other IL methods, retaining RTMPC’s robustness and performance. The prediction horizon used is $N = 20$, and the DNN input size is adjusted accordingly.

Performance and Training Time), with the difference that performance is based on the stage cost of the ancillary NMPC Eq. (16).

Training Details As in Section VII, training is performed by collecting demonstrations with the multirotor starting from slightly different initial states inside the tube centered around the origin. The nominal flip maneuver is pre-generated, as the goal state $\mathbf{x}_{t_0}^e$ (with $t_0 = 0$) does not change, and only the ancillary NMPC is solved at every timestep. The resulting flip maneuver takes about $T_f = 2.5\text{s}$, and demonstrations are collected over an episode of length 3.0s, at 50Hz ($T = 150$ environment steps per demonstration). To speed-up the demonstration collection phase, and thereby avoid excessive re-training of the policy, we collect demonstrations in batches for all the baselines, using 10 demonstrations per batch for 20 batches. For SA-methods, we collect demonstrations one-by-one, and we implement the fine-tuning procedure described in Section V-D by performing DA with the first collected demonstration, while we do not perform DA for the following demonstrations. Because of its computational efficiency, we always use the sensitivity-based DA (i.e., Eq. (19), assuming no changes in active set of constraints). Each time the policy is updated, we evaluate it 20 times in source \mathcal{S} and target \mathcal{T} environments. The evaluations are averaged across 10 different random seeds. To further speed-up training of all the methods, we update the previously trained policy using only the newly collected batch of demonstrations (or single demonstration, for SA). All the policies are trained using the ADAM optimizer for up to 400 epochs, but we terminate training if the validation loss (from 30% of the data) does not decrease within 30 epochs. Last, to study the effects of varying the number of samples used for DA, we introduce SA- N_S , a variant of SA where we sample uniformly inside the tube $N_S = \{25, 50, 100\}$ samples for every timestep.

B. Numerical Evaluation of Robustness, Performance, and Efficiency

Comparison with Baselines. We start by evaluating the robustness and performance of the proposed approach as a function of the number of demonstrations collected in simulation, and as a function of the training time.

Fig. 11 shows the robustness of the considered method as a function of the number of expert demonstrations. It reveals that SA-based approaches can achieve full success rate in the environment with disturbances (target, \mathcal{T}) and without disturbances (source, \mathcal{S}) after a single demonstration, while the best-performing baseline, DAGger+DR, requires about 60 demonstrations to achieve full robustness in \mathcal{S} , and more than 100 in \mathcal{T} . SA-based methods, therefore, enable more than one order of magnitude reduction in the number of demonstrations (interactions with the environment) compared to DAGger+DR. As previously observed in Section VII, DAGger alone is not robust. Additionally, BC methods fail to converge, potentially due to the lack of sufficiently meaningful exploration and the forgetting caused by the iterative training strategy employed.

Fig. 12 additionally shows the robustness as a function of the training time (recall, this includes demonstration collection and

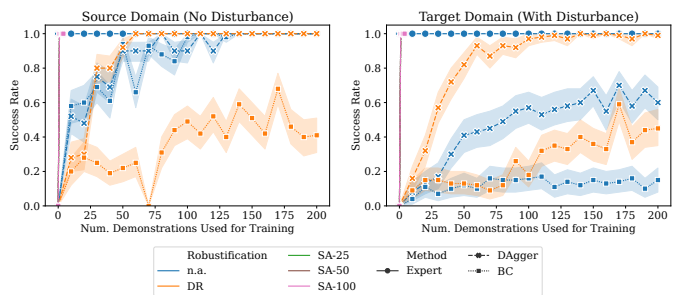


Fig. 11: Robustness as a function of the number of training demonstrations. The IL methods that use the proposed DA strategy, Sampling-Augmentation (SA), overlap on the top-left part of the diagram, achieving full success rate in both the source and target domain of the training environment. Uncertainties in the target domains are applied in the form of a constant external force acting on the center of mass of the multirotor, representing large wind disturbances.

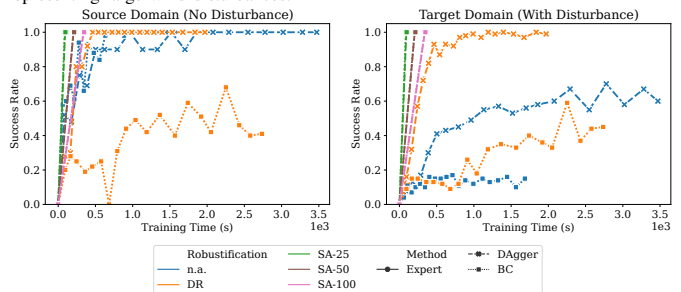


Fig. 12: Robustness as a function of the training time. The IL methods that use the proposed DA and fine-tuning strategy, Sampling-Augmentation (SA), achieve full robustness under uncertainties in a fraction of the training time required by the best performing robust baseline, DAGger + DR.

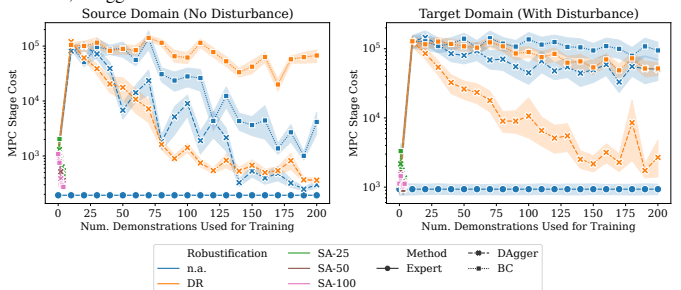


Fig. 13: Performance as a function of the number of training demonstrations. The IL methods that use the proposed DA and fine-tuning strategy, Sampling-Augmentation (SA), achieve performance close to the expert in less than 10 demonstrations, while the best-performing baseline, DAGger + DR, achieves comparable performance but in a larger number of demonstrations.

policy train). The results show that the demonstration-efficiency of SA-based methods translates into significant improvements in training time, as DAGger+DR requires more than 3 times the training time than SA-based approaches. These improvements are larger for the variants of SA that generate fewer extra samples (e.g., SA-25).

Last, Fig. 13 reports the *performance* as a function of the number of demonstrations. The results indicate that SA-based methods can achieve low tracking errors even after a single demonstration. Furthermore, employing a fine-tuning phase (after the initial demonstration) proves highly advantageous in further reducing this error, thereby reducing the performance gap between policies obtained via SA and the expert.

Comparison of Sampling Strategies. Table V provides a detailed comparison of performance, robustness, and training time of the different variants of SA methods, as a function of the number of demonstrations (1, 2 and 10), and compares those

TABLE IV: Computation time required to generated a new action for the nonlinear RTMPC (Expert) and the proposed learned DNN policy (Policy). The policy is 66.1 times faster than the optimization-based expert. Evaluation performed on an Intel i9-10920. We note that the faster inference time than the linear case is caused by the input dimension being smaller (14 vs 188)

Method	Setup	Time (ms)			
		Mean	St. Dev.	Min	Max
Expert (Nonlinear)	ACADOS [53]	7.28	0.15	7.05	8.00
Policy	PyTorch	0.11	0.01	0.11	0.27

Method	Robustif.	# of Demonstr.	Robustness success rate (%. \uparrow)				Performance expert gap (%. \downarrow)				Efficiency training time (s. \downarrow)	
			S		T		S		T		-	
			mean	std	mean	std	mean	std	mean	std	mean	std
Dagger	DR	50	92	27	82	39	9094	20608	3096	5497	392	34
		100	100	0	97	17	634	711	1277	4947	810	104
		200	100	0	99	10	91	73	274	1247	1970	154
BC	SA-sparse (18)	1	100	0	100	0	553	462	211	228	84	9
		2	100	0	97	17	41	39	371	1808	88	10
		10	100	0	97	17	33	42	226	815	115	10
		1	100	0	100	0	956	402	270	384	87	15
		2	100	0	100	0	148	140	107	150	90	14
		10	100	0	100	0	107	175	90	83	117	14
	SA-50	1	100	0	100	0	421	193	105	116	204	32
		2	100	0	100	0	76	31	66	56	207	31
		10	100	0	100	0	55	28	76	102	235	31
		1	100	0	100	0	291	154	89	105	339	72
	SA-100	2	100	0	100	0	57	20	76	85	342	72
		1	100	0	100	0	33	21	97	118	369	72
10		100	0	100	0	30	28	90	109	373	29	
10		100	0	100	0	30	28	90	109	373	29	
Dagger	SA-sparse (18)	1	100	0	100	0	747	705	319	879	85	6
		2	100	0	100	0	222	122	142	219	89	6
		10	100	0	100	0	29	24	114	150	117	6
		1	100	0	100	0	579	224	160	168	92	12
		2	100	0	100	0	366	279	122	182	96	12
		10	100	0	100	0	110	115	100	120	124	12
	SA-50	1	100	0	100	0	361	161	78	91	206	28
		2	100	0	100	0	169	117	77	80	210	28
		10	100	0	100	0	56	77	82	107	237	28
		1	100	0	100	0	309	133	92	105	342	29
	SA-100	2	100	0	100	0	100	61	77	96	346	29
		1	100	0	100	0	30	28	90	109	373	29
10		100	0	100	0	30	28	90	109	373	29	
10		100	0	100	0	30	28	90	109	373	29	

TABLE V: Performance, robustness and training time for SA-based methods after 1, 2, and 10 demonstrations, compared with the best performing baselines, Dagger+DR, in the environment without disturbances (S , source), and with (T , target). Robustness is color-coded from white (100%) to red (90% or below). Performance and training time are color-coded from green (fast training time, small expert gap) to red (long training time, large expert gap). The results highlight that SA-methods achieve high robustness and close to expert performance compared to Dagger+DR, even after a single demonstration, and their performance can be further improved via additional fine-tuning demonstrations. We note that Dagger and BC-based approaches differ at one demonstration due to non-determinism in the training procedure.

with the best-performing baselines, Dagger+DR. As expected, SA methods that require fewer samples obtain significant improvements in training time, while increasing the number of samples is beneficial in reducing the mean and the variance of the expert gap, both with and without disturbances. Table V additionally highlights the benefits of fine-tuning, as even methods that use few samples (e.g., SA-sparse, SA-25) can obtain a significant performance improvement after a single fine-tuning demonstration (2 demonstrations in total), while there are diminishing returns for additional fine-tuning demonstrations (e.g., 10 demonstrations).

Computation. The computational cost of the nonlinear RTMPC expert and the learned policy is reported in Table IV, highlighting that the policy is 66 times faster than the expert. The average time to step the training environment is 2.1 ms.

C. Hardware Evaluation

We experimentally evaluate the ability of the policy to perform a flip on a real multirotor, under real-world uncertainties such as model errors (e.g., inaccurate thrust to battery voltage mappings, aerodynamic coefficients, moments of inertia) and external disturbances (e.g., ground effect). The tested policy is obtained using Dagger+SA-25 trained after 2 demonstrations (the first with DA, the second for fine-tuning), as the method

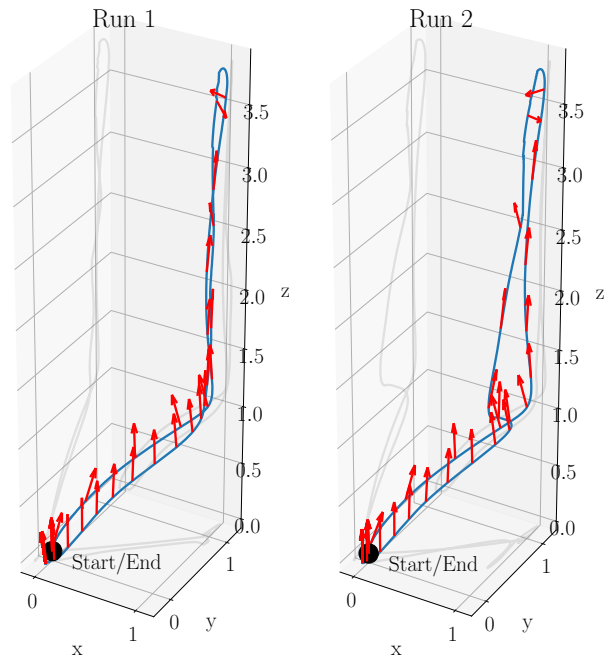


Fig. 14: Acrobatic flip trajectory performed by our UAV using a policy efficiently learned from a nonlinear Robust Tube MPC. All the units are expressed in meters. The red arrows denote the direction of the thrust vector on the quadrotor, and they highlight that the flip occurs at the point of highest altitude of the maneuver. The plot shows the additional take-off/landing phase, also performed by the learned policy, taking the robot back and forth the origin and $(x, y, z) = (1, 1, 1)$, that is the point where the flip starts and ends. All the units are expressed in (m).

represents a good trade-off between performance, robustness and training time. As in Section VII, we deploy the learned policy on an onboard Nvidia Jetson TX2, where it runs at 100Hz. The maneuver includes a take-off/landing phase consisting of a 1m ramp on x - y - z in W and overall has a total duration of 6s. The maneuver is repeated 5 times in a row, to demonstrate repeatability, recording successful execution of the maneuver and successful landing at the designated location in all the cases. Fig. 1 shows a time-lapse of the different phases of the maneuver (excluding the ramp from and to the landing location). The 3D position of the robot, as well as the direction of its thrust vector, are shown for two runs in Fig. 14, highlighting the large distance and altitude traveled in a short time. Fig. 15 additionally shows some critical parameters of the maneuvers, such as the attitude and the angular velocity, as well as thrust and the vertical velocities. It highlights that the robot rotates at up to 11rad/s, and the overall 360° rotation takes about 0.5s. Overall, these results validate our numerical analysis and highlight the robustness and performance of a policy efficiently trained from 2 demonstrations and about 100s of training time. Our video submission [57] includes an additional experiment demonstrating near-minimum time navigation from one position to another, starting and ending with velocity close to zero, using a policy trained with two demonstrations (Dagger+SA-25).

IX. DISCUSSION AND CONCLUSION

This work has presented an IL strategy to efficiently train a robust DNN policy from MPC. Key ideas of our work were to (a) leverage a Robust Tube variant of MPC, called RTMPC, to collect demonstrations using existing IL methods (Dagger,

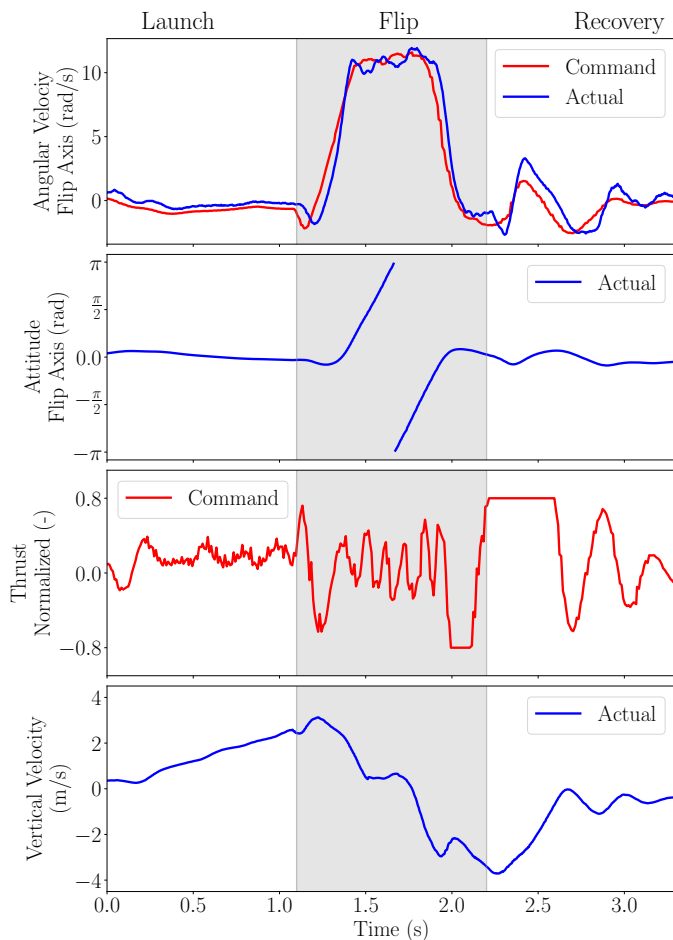


Fig. 15: Control inputs generated by the learned policy and relevant states during the real-world acrobatic flip maneuver on a multirotor, where the robot is subject to large levels of uncertainties, caused primarily by model mismatches such as thrust-to-battery voltage mappings and hard-to-model aerodynamic effects. Despite the large level of uncertainties, that require the usage of the maximum thrust allowed, the maneuver is completed successfully, and the robot reaches the desired vertical velocity of -1.0 m s^{-1} at the end of the recovery phase (and that corresponds to the initial velocity of the landing phase). We highlight that the flip is performed at an angular velocity of about 11.0 rad/s . The actual thrust t_{cmd} can be related to the normalized thrust \bar{t}_{cmd} via $t_{\text{cmd}} = mg(1 + \bar{t}_{\text{cmd}})$, where mg is the weight force of the robot.

BC), and (b) to augment the collected demonstrations with extra state-and-actions sampled from the robust control invariant set (tube) of the controller, leveraging the key intuition that the tube represents an approximation of the support of the state distribution that the learned policy will encounter at deployment, when subject to uncertainties. We first demonstrate these properties by efficiently training a policy that enables robust trajectory tracking on a multirotor operating at near-hover conditions. This is accomplished by leveraging a linear model of the robot and a linear RTMPC framework. Our numerical and experimental evaluations highlight the possibility of training a policy robust to real-world uncertainties (such as wind and model errors) after a single demonstration, collected either in simulation or directly with the real robot.

While obtaining extra data in a computationally efficient way is straightforward in a linear RTMPC setting, since actions can be computed efficiently using the linear ancillary controller, as shown in our conference paper [19], the same efficiency can be challenging to achieve when leveraging nonlinear

variants of RTMPC. Therefore, in this journal extension of [19] we have presented a strategy to efficiently perform tube-guided DA when leveraging nonlinear variants of RTMPC. The key idea, in this case, was to perform DA by generating a linear approximation of the ancillary NMPC employed to maintain the system under uncertainties inside the tube. We have additionally presented a fine-tuning phase that requires very few demonstrations and can significantly reduce the errors introduced by the approximation of the ancillary NMPC. Experimental evaluations on the challenging task of performing a flip on a multirotor have demonstrated the performance of policies trained with only two demonstrations, requiring less than one-third of the training time needed by existing methods.

While design procedures to accurately estimate tubes given uncertainty and model priors may be complex and computationally expensive, our work has also demonstrated that fixed-size approximations of the tube are sufficient to efficiently generate policies that can withstand real-world uncertainties. Additionally, depending on the scenario, designing a tube and performing tube-guided DA may be a simpler method to learn robust policies compared to strategies based on DR, where a user needs to carefully randomize relevant environmental parameters. This is the case, for example, when learning tubes from data, i.e., when prior knowledge on the state deviations caused by uncertainties is known, but the exact sources of those uncertainties are unknown, and therefore it is hard to identify what are the parameters that should be randomized in the popular DR procedures.

Overall, our work has demonstrated that it is possible to efficiently generate high-quality, robust policies from MPC, i.e. in a way that requires few (a) queries to expensive optimal controllers, and (b) environment interactions. This can have important repercussions across different fields of robotics. For example, the improvements in (a) enable speed-up in the training time of policies, a convenient property when performing controller tuning or when working on robots where the model is so poorly known that the model/controller/policy needs to be modified whenever new data (e.g., obtained from the previous deployment of the learned policy) becomes available. Additionally, the improvements in (b) can open up further opportunities to imitation-learn robust policies in environments that are extremely expensive to query, such as the real world (where expensive is intended in terms of effort to run data collection), or in scenarios where the simulated environments require a large amount of computation (i.e., in fluid-dynamic simulations). Last, shifting gear from the IL setting, we would like to highlight that our proposed efficient policy learning procedure can serve as a bootstrapping methodology, leveraging *model and uncertainty priors*, to *efficiently* obtain *high-performance, robust* initial policy guesses for subsequent policy fine-tuning steps using model-free methods, such as Reinforcement Learning (RL), with the potential to significantly reduce the amount of random exploration typically required by these methods.

X. ACKNOWLEDGMENTS

We thank Kota Kondo for the help with the experimental evaluation, Prof. Michael Everett, Dr. Dong-Ki Kim, Tong Zhao and Dr. Donggun Lee for feedback and discussions.

REFERENCES

- [1] F. Borrelli, A. Bemporad, and M. Morari, *Predictive control for linear and hybrid systems*. Cambridge University Press, 2017.
- [2] J. B. Rawlings, D. Q. Mayne, and M. Diehl, *Model predictive control: theory, computation, and design*. Nob Hill Publishing Madison, WI, 2017, vol. 2.
- [3] B. T. Lopez, J.-J. E. Slotine, and J. P. How, “Dynamic tube MPC for nonlinear systems,” in *2019 American Control Conference (ACC)*. IEEE, 2019, pp. 1655–1662.
- [4] B. T. Lopez, “Adaptive robust model predictive control for nonlinear systems,” Ph.D. dissertation, Massachusetts Institute of Technology, 2019.
- [5] W. Li and E. Todorov, “Iterative linear quadratic regulator design for nonlinear biological movement systems,” in *ICINCO (1)*. Citeseer, 2004, pp. 222–229.
- [6] M. Kamel, M. Burri, and R. Siegwart, “Linear vs nonlinear MPC for trajectory tracking applied to rotary wing micro aerial vehicles,” *IFAC-PapersOnLine*, vol. 50, no. 1, pp. 3463–3469, 2017.
- [7] M. V. Minniti, F. Farshidian, R. Grandia, and M. Hutter, “Whole-body MPC for a dynamically stable mobile manipulator,” *IEEE Robotics and Automation Letters*, vol. 4, no. 4, pp. 3687–3694, 2019.
- [8] G. Williams, P. Drews, B. Goldfain, J. M. Rehg, and E. A. Theodorou, “Aggressive driving with model predictive path integral control,” in *2016 IEEE International Conference on Robotics and Automation (ICRA)*. IEEE, 2016, pp. 1433–1440.
- [9] J. B. Rawling and P. Kumar, “Industrial, large-scale model predictive control with deep neural networks,” http://helper.ipam.ucla.edu/publications/lco2020/lco2020_16406.pdf, (Accessed on 05/18/2021).
- [10] E. Kaufmann, A. Loquercio, R. Ranftl, M. Müller, V. Koltun, and D. Scaramuzza, “Deep drone acrobatics,” *Robotics, Science, and Systems (RSS)*, 2020.
- [11] S. Ross, N. Melik-Barkhudarov, K. S. Shankar, A. Wendel, D. Dey, J. A. Bagnell, and M. Hebert, “Learning monocular reactive uav control in cluttered natural environments,” in *2013 IEEE international conference on robotics and automation*. IEEE, 2013, pp. 1765–1772.
- [12] A. Reske, J. Carius, Y. Ma, F. Farshidian, and M. Hutter, “Imitation learning from MPC for quadrupedal multi-gait control,” in *2021 IEEE International Conference on Robotics and Automation (ICRA)*. IEEE, 2021, pp. 5014–5020.
- [13] D. A. Pomerleau, “Alvin: An autonomous land vehicle in a neural network,” Carnegie-Mellon Univ Pittsburgh PA Artificial Intelligence and Psychology, Tech. Rep., 1989.
- [14] T. Osa, J. Pajarinen, G. Neumann, J. A. Bagnell, P. Abbeel, and J. Peters, “An algorithmic perspective on imitation learning,” *arXiv preprint arXiv:1811.06711*, 2018.
- [15] M. Bojarski, D. Del Testa, D. Dworakowski, B. Firner, B. Flepp, P. Goyal, L. D. Jackel, M. Monfort, U. Muller, J. Zhang *et al.*, “End to end learning for self-driving cars,” *arXiv preprint arXiv:1604.07316*, 2016.
- [16] S. Ross, G. Gordon, and D. Bagnell, “A reduction of imitation learning and structured prediction to no-regret online learning,” in *Proceedings of the fourteenth international conference on artificial intelligence and statistics*. JMLR Workshop and Conference Proceedings, 2011, pp. 627–635.
- [17] X. B. Peng, M. Andrychowicz, W. Zaremba, and P. Abbeel, “Sim-to-real transfer of robotic control with dynamics randomization,” in *2018 IEEE international conference on robotics and automation (ICRA)*. IEEE, 2018, pp. 3803–3810.
- [18] A. Loquercio, E. Kaufmann, R. Ranftl, A. Dosovitskiy, V. Koltun, and D. Scaramuzza, “Deep drone racing: From simulation to reality with domain randomization,” *IEEE Transactions on Robotics*, vol. 36, no. 1, pp. 1–14, 2019.
- [19] A. Tagliabue, D.-K. Kim, M. Everett, and J. P. How, “Demonstration-efficient guided policy search via imitation of robust tube MPC,” in *2022 International Conference on Robotics and Automation (ICRA)*. IEEE, 2022, pp. 462–468.
- [20] X. Zhang, M. Bujarbaruah, and F. Borrelli, “Near-optimal rapid MPC using neural networks: A primal-dual policy learning framework,” *IEEE Transactions on Control Systems Technology*, 2020.
- [21] M. Hertneck, J. Köhler, S. Trimpe, and F. Allgöwer, “Learning an approximate model predictive controller with guarantees,” *IEEE Control Systems Letters*, vol. 2, no. 3, pp. 543–548, 2018.
- [22] S. Chen, K. Saulnier, N. Atanasov, D. D. Lee, V. Kumar, G. J. Pappas, and M. Morari, “Approximating explicit model predictive control using constrained neural networks,” in *2018 Annual American control conference (ACC)*. IEEE, 2018, pp. 1520–1527.
- [23] S. W. Chen, T. Wang, N. Atanasov, V. Kumar, and M. Morari, “Large scale model predictive control with neural networks and primal active sets,” *Automatica*, vol. 135, p. 109947, 2022.
- [24] Y. Pan, C.-A. Cheng, K. Saigol, K. Lee, X. Yan, E. A. Theodorou, and B. Boots, “Imitation learning for agile autonomous driving,” *The International Journal of Robotics Research*, vol. 39, no. 2-3, pp. 286–302, 2020.
- [25] D. H. Jacobson and D. Q. Mayne, *Differential dynamic programming*. Elsevier Publishing Company, 1970, no. 24.
- [26] S. Levine and V. Koltun, “Guided policy search,” in *International conference on machine learning*. PMLR, 2013, pp. 1–9.
- [27] T. Zhang, G. Kahn, S. Levine, and P. Abbeel, “Learning deep control policies for autonomous aerial vehicles with MPC-guided policy search,” in *2016 IEEE international conference on robotics and automation (ICRA)*. IEEE, 2016, pp. 528–535.
- [28] G. Kahn, T. Zhang, S. Levine, and P. Abbeel, “Plato: Policy learning using adaptive trajectory optimization,” in *2017 IEEE International Conference on Robotics and Automation (ICRA)*. IEEE, 2017, pp. 3342–3349.
- [29] J. Carius, F. Farshidian, and M. Hutter, “MPC-net: A first principles guided policy search,” *IEEE Robotics and Automation Letters*, vol. 5, no. 2, pp. 2897–2904, 2020.
- [30] A. Farchy, S. Barrett, P. MacAlpine, and P. Stone, “Humanoid robots learning to walk faster: From the real world to simulation and back,” in *Proceedings of the 2013 international conference on Autonomous agents and multi-agent systems*, 2013, pp. 39–46.
- [31] Y. Chebotar, A. Handa, V. Makoviychuk, M. Macklin, J. Issac, N. Ratliff, and D. Fox, “Closing the sim-to-real loop: Adapting simulation randomization with real world experience,” in *2019 International Conference on Robotics and Automation (ICRA)*. IEEE, 2019, pp. 8973–8979.
- [32] M. Laskey, J. Lee, R. Fox, A. Dragan, and K. Goldberg, “Dart: Noise injection for robust imitation learning,” in *Conference on robot learning*. PMLR, 2017, pp. 143–156.
- [33] J. Hanna and P. Stone, “Grounded action transformation for robot learning in simulation,” in *Proceedings of the AAAI Conference on Artificial Intelligence*, vol. 31, no. 1, 2017.
- [34] S. Desai, I. Durugkar, H. Karnan, G. Warnell, J. Hanna, P. Stone, and A. Sony, “An imitation from observation approach to transfer learning with dynamics mismatch,” *Advances in Neural Information Processing Systems*, vol. 33, 2020.
- [35] D. Q. Mayne, M. M. Seron, and S. Raković, “Robust model predictive control of constrained linear systems with bounded disturbances,” *Automatica*, vol. 41, no. 2, pp. 219–224, 2005.
- [36] D. Q. Mayne, E. C. Kerrigan, E. Van Wyk, and P. Falugi, “Tube-based robust nonlinear model predictive control,” *International journal of robust and nonlinear control*, vol. 21, no. 11, pp. 1341–1353, 2011.
- [37] H. Tsukamoto and S.-J. Chung, “Learning-based robust motion planning with guaranteed stability: A contraction theory approach,” *IEEE Robotics and Automation Letters*, 2021.
- [38] —, “Neural contraction metrics for robust estimation and control: A convex optimization approach,” *IEEE Control Systems Letters*, vol. 5, no. 1, pp. 211–216, 2020.
- [39] D. Krishnamoorthy, “A sensitivity-based data augmentation framework for model predictive control policy approximation,” *IEEE Transactions on Automatic Control*, vol. 67, no. 11, pp. 6090–6097, 2022.
- [40] —, “An improved data augmentation scheme for model predictive control policy approximation,” *arXiv preprint arXiv:2303.05607*, 2023.
- [41] R. S. Sutton and A. G. Barto, *Reinforcement learning: An introduction*. MIT press, 2018.
- [42] K. J. Åström and R. M. Murray, *Feedback systems: an introduction for scientists and engineers*. Princeton university press, 2021.
- [43] M. Kamel, T. Stastny, K. Alexis, and R. Siegwart, “Model predictive control for trajectory tracking of unmanned aerial vehicles using robot operating system,” in *Robot operating system (ROS)*. Springer, 2017, pp. 3–39.
- [44] D. D. Fan, A.-a. Agha-mohammadi, and E. A. Theodorou, “Deep learning tubes for tube MPC,” *arXiv preprint arXiv:2002.01587*, 2020.
- [45] W. M. Kouw and M. Loog, “An introduction to domain adaptation and transfer learning,” *arXiv preprint arXiv:1812.11806*, 2018.
- [46] M. Diehl, “Real-time optimization for large scale nonlinear processes,” Ph.D. dissertation, Heidelberg University, 2001.
- [47] T. Lee, “Geometric tracking control of the attitude dynamics of a rigid body on so(3),” in *Proceedings of the 2011 American Control Conference*, 2011, pp. 1200–1205.
- [48] M. W. Mueller, M. Hehn, and R. D’Andrea, “A computationally efficient algorithm for state-to-state quadcopter trajectory generation and feasibility verification,” in *2013 IEEE/RSJ International Conference on Intelligent Robots and Systems*. IEEE, 2013, pp. 3480–3486.

- [49] M. D. Shuster *et al.*, “A survey of attitude representations,” *Navigation*, vol. 8, no. 9, pp. 439–517, 1993.
- [50] D. P. Kingma and J. Ba, “Adam: A method for stochastic optimization,” *arXiv preprint arXiv:1412.6980*, 2014.
- [51] S. Diamond and S. Boyd, “CVXPY: A Python-embedded modeling language for convex optimization,” *Journal of Machine Learning Research*, vol. 17, no. 83, pp. 1–5, 2016.
- [52] Aerospace Controls Laboratory, “snap-stack: Autopilot code and host tools for flying snapdragon flight-based vehicles,” <https://gitlab.com/mit-acl/fsw/snap-stack>, (Accessed on 02/23/2020).
- [53] R. Verschueren, G. Frison, D. Kouzoupis, J. Frey, N. van Duijkeren, A. Zanelli, B. Novoselnik, T. Albin, R. Quirynen, and M. Diehl, “acados – a modular open-source framework for fast embedded optimal control,” *Mathematical Programming Computation*, Oct 2021. [Online]. Available: <https://doi.org/10.1007/s12532-021-00208-8>
- [54] G. Frison and M. Diehl, “Hpipm: a high-performance quadratic programming framework for model predictive control,” *IFAC-PapersOnLine*, vol. 53, no. 2, pp. 6563–6569, 2020.
- [55] J. Gillis, B. Vandewal, G. Pipeleers, and J. Swevers, “Effortless modeling of optimal control problems with rokit,” in *39th Benelux Meeting on Systems and Control, Date: 2020/03/10-2020/03/12, Location: Elspeet, The Netherlands*, 2020.
- [56] T. Kusaka and T. Tanaka, “Stateful rotor for continuity of quaternion and fast sensor fusion algorithm using 9-axis sensors,” *Sensors*, vol. 22, no. 20, p. 7989, 2022.
- [57] [Online]. Available: <https://youtu.be/aWRuvy3LviI>